Functional screenings reveal different requirements for host microRNAs in *Salmonella* and *Shigella* infection

Carmen Aguilar[1,9], Ana Rita Cruz[2,9], Ines Rodrigues Lopes[2,3], Claire Maudet[1,6], Ushasree Sunkavalli[1], Ricardo Jorge Silva[2], Malvika Sharan[1,7], Clivia Lisowski[1], Sara Zaldívar-López[4], Juan José Garrido[4], Mauro Giacca[5,8], Miguel Mano[2*] and Ana Eulalio[1,3*]

MicroRNAs (miRNAs) are increasingly recognized for their role in infection by bacterial pathogens, although the effect of each individual miRNA remains largely unknown. Here, we used a comparative genome-wide microscopy-based functional screening approach to identify miRNAs controlling infection by two bacterial pathogens—*Salmonella enterica* serovar Typhimurium and *Shigella flexneri*. Despite the similarities between these pathogens, we found infections to be controlled by largely non-overlapping subsets of miRNAs, seemingly reflecting different requirements prompted by their distinct intracellular lifestyles. By characterizing a small subset of miRNAs chosen among the strongest inhibitors of *Shigella* infection, we discovered that miR-3668, miR-4732-5p and miR-6073 exert a selective effect on *Shigella* infection by impairing bacterial actin-based motility by downregulating N-WASP. Additionally, by identifying let-7i-3p miRNA as a strong inhibitor of *Salmonella* replication and performing in-depth analysis of its mechanisms of action, we showed that this miRNA specifically inhibits *Salmonella* infection via modulation of endolysosomal trafficking and the vacuolar environment by targeting the host RGS2 protein. These findings illustrate two paradigms underlying miRNA-mediated regulation of bacterial infection, acting as part of the host response to infection, or as part of bacterial strategies to modulate the host environment and favour pathogenesis.

MicroRNAs (miRNAs) have a pivotal role as post-transcriptional regulators of gene expression in a wide range of organisms[1]. Target mRNA repression occurs through translational inhibition and mRNA degradation[2]. Despite their relative low number (approximately 2,500 human mature miRNAs are currently annotated), each individual miRNA can regulate hundreds of targets; it is estimated that around 60% of the human transcriptome is regulated by the miRNome[3].

Taking into consideration the pervasive regulatory role of the miRNome and bacterial dependency on host processes, it is not surprising that miRNAs have emerged as having important roles in the interaction between mammalian hosts and bacterial pathogens[4,5]. Notably, miRNA regulation has been shown to be both integral to the host immune response to control infection and a strategy that is hijacked by bacteria to promote infection. The study of miRNAs in the context of bacterial infection has provided important insights into the current understanding of host pathways relevant for infection by various pathogens. Nonetheless, the functions of the majority of miRNAs have not been fully characterized. The application of high-throughput screening approaches using genome-wide libraries of synthetic miRNAs, enabling systematic functional analysis of individual miRNAs, is a valuable strategy to achieve this goal[6–8]. Indeed, miRNA screenings have been successfully applied to several fields of biomedical research[9–12]. We previously applied this approach to the study of miRNAs in bacterial pathogen infection, specifically *Salmonella enterica* serovar Typhimurium (hereafter, *Salmonella*)[13]. In this proof-of-principle study, we identified the miR-15 miRNA family as a restriction factor for *Salmonella* infection, uncovering a previously uncharacterized link between *Salmonella* and the host cell cycle.

Here, we applied a comparative microscopy-based high-throughput screening approach with a genome-wide library of miRNA mimics to identify those controlling infection of epithelial cells by two important enteric bacterial pathogens—*Salmonella* and *Shigella flexneri* (hereafter, *Shigella*)[14–16]. We selected these two pathogens as archetypes of intracellular bacteria, considering their divergent intracellular lifestyles despite being closely related. Following invasion, *Salmonella* replication occurs, to a large extent, confined to a vacuolar structure (the *Salmonella*-containing vacuole[17] (SCV)) whereas *Shigella* rapidly escapes the vacuole and replicates exclusively in the cytoplasm[18]. In addition, *Shigella* exploits actin-based motility for intracellular and cell-to-cell spreading, a feature absent in *Salmonella*[19]. We reasoned that the comparison of miRNAs controlling infection by these bacteria would enable identification of host cellular factors and/or pathways relevant for their dissimilar intracellular lifestyles. Indeed, we found that miRNAs regulate various stages of infection, and that largely non-overlapping miRNA subsets regulate infection by these pathogens. Furthermore, we report two examples that illustrate the validity of this unbiased

[1]Host RNA Metabolism Group, Institute for Molecular Infection Biology (IMIB), University of Würzburg, Würzburg, Germany. [2]Functional Genomics and RNA-based Therapeutics Laboratory, Center for Neuroscience and Cell Biology (CNC), University of Coimbra, Coimbra, Portugal. [3]RNA and Infection Laboratory, Center for Neuroscience and Cell Biology (CNC), University of Coimbra, Coimbra, Portugal. [4]Grupo de Genómica y Mejora Animal, Departamento de Genética, Facultad de Veterinaria, Universidad de Córdoba, Córdoba, Spain. [5]Molecular Medicine Laboratory, International Centre for Genetic Engineering and Biotechnology (ICGEB), Trieste, Italy. [6]Present address: Biology of Infection Unit, Institut Pasteur, Paris, France. [7]Present address: European Molecular Biology Laboratory (EMBL), Heidelberg, Germany. [8]Present address: School of Cardiovascular Medicine and Science, King's College London, London, UK. [9]These authors contributed equally: Carmen Aguilar, Ana Rita Cruz. *e-mail: mano@ci.uc.pt; ana.eulalio@uni-wuerzburg.de; aeulalio@ci.uc.pt

screening approach to provide relevant biological information. Collectively, this work demonstrates that the systematic identification of miRNAs and downstream targets is a powerful strategy for investigating the complexity of host–pathogen crosstalk.

Results

miRNAs are important regulators of *Salmonella* and *Shigella* infection. To systematically and comprehensively identify miRNAs modulating infection by two bacterial pathogens—*Salmonella* and *Shigella*—we performed high-throughput fluorescence microscopy-based screenings using a library of miRNA mimics (miRBase 19, comprising 2,042 mature miRNAs; Fig. 1a). HeLa cells, an epithelial cell line commonly used to study infection by these pathogens, was selected as a cellular model. Cells were transfected with the miRNA library and infected with *Salmonella* or *Shigella*; infection was analysed by fluorescence microscopy at late times after infection (20 h post-infection (hpi) for *Salmonella*; 6 hpi for *Shigella*). Automated image analysis extracted multiple features, including host cell count and number of infected cells (Extended Data Fig. 1a). Screening results are presented compared with control miRNA, considering the percentage of cells with replicating bacteria (Fig. 1b,d and Supplementary Tables 1 and 2). Three independent experiments were performed for the screenings, showing very good reproducibility (Spearman's $r > 0.7$; Extended Data Fig. 1b,c); miRNAs decreasing cell viability (<65%) were excluded (481 and 494 miRNAs for *Salmonella* and *Shigella* screenings, respectively).

Of the 1,561 miRNAs considered for analysis from the *Salmonella* screening, 84 and 53 significantly decreased and increased infection by at least twofold, respectively ($P < 0.05$; Fig. 1b and Supplementary Table 1); from the 1,548 miRNAs selected from the *Shigella* screening, 44 and 157 significantly decreased and increased infection by at least twofold, respectively ($P < 0.05$; Fig. 1d and Supplementary Table 2). Images of the three highest-ranking miRNAs increasing or decreasing *Salmonella* and *Shigella* infection are shown in Fig. 1c,e.

Comparison of the two screenings revealed a weak correlation (Spearman's $r = 0.352$; Fig. 1f). Indeed, only 16 miRNAs increased, and 7 miRNAs decreased infection by both pathogens by more than twofold. Images illustrating the various regulation paradigms are shown in Fig. 1g.

Overall, these results position host miRNAs as strong regulators of *Salmonella* and *Shigella* infection, and underline a high degree of selectivity of miRNA action towards a specific pathogen.

miRNAs regulate different stages of bacterial infection. To further validate and characterize the miRNAs that strongly modulated *Salmonella* and/or *Shigella* infection, we determined the effects of each miRNA at early (binding, 0.5 hpi, *Shigella*; binding, 4 hpi, *Salmonella*), intermediate (3 hpi, *Shigella*; 8 hpi, *Salmonella*) and late (6 hpi, *Shigella*; 20 hpi, *Salmonella*) stages of infection (Fig. 2a). This analysis was performed for the 55 miRNAs that affected *Salmonella* infection by at least 2.5-fold in the initial screening (39 miRNAs decreased indection and 16 miRNAs increased infection; Fig. 2a, green) and the 41 miRNAs that affected *Shigella* infection by at least threefold (12 miRNAs decreased infection and 29 miRNAs increased infection; Fig. 2a, orange). Analysis was extended to 7 miRNAs that decreased infection and 16 miRNAs that increased infection of both pathogens by at least twofold (Fig. 2a, pink). In addition, we included the seven miRNAs that decreased *Salmonella* infection but increased *Shigella* infection by at least twofold (Fig. 2a, blue), and the two miRNAs with the reciprocal phenotype (Fig. 2a, yellow). Overall, 110 miRNAs were tested in time-course experiments, 74 were selected for their effect on *Salmonella* infection and 66 were selected for their effect on *Shigella* infection. Of these, the phenotypes of 70 and 62 miRNAs (94–95%) were successfully validated for their effects on *Salmonella* and *Shigella* infection, respectively (Extended Data Fig. 1d,e).

Analysis of the time-course experiments revealed that 12 and 33 miRNAs affected *Salmonella* or *Shigella* binding, respectively, by at least twofold (Fig. 2a). A strong correlation was observed between miRNAs affecting binding and the first time point tested after bacterial internalization (Fig. 2b,d). A group of miRNAs predominantly affected intermediate and late stages of infection, suggesting an action on bacterial intracellular replication (Fig. 2a,c,e).

Overall, these results reveal that different stages of the bacterial infection cycle are affected by specific miRNAs. Thus, miRNA modulation might prove useful to pinpoint requirements of host cell functions for different infection stages.

miR-3668, miR-4732-5p and miR-6073 strongly inhibit *Shigella* intercellular spreading. Among the strongest inhibitors of *Shigella* infection were miR-3668, miR-4732-5p and miR-6073. Notably, these miRNAs did not affect *Shigella* binding, but markedly reduced the percentage of infected cells at intermediate and late times after infection (3 and 6 hpi; Fig. 2a). Microscopic analysis showed that miR-3668, miR-4732-5p and miR-6073 confined infection to a small number of cells with high bacterial load (Fig. 3a), suggesting a strong interference with *Shigella* intercellular spreading. Analysis of infection foci area confirmed this hypothesis (14–19% of control; Fig. 3c). The effects of the three miRNAs were similar to that observed for the spreading-deficient *Shigella* Δ*icsA* mutant (12% of control; Fig. 3c). This marked defect in spreading was corroborated by time-lapse microscopy (Supplementary Videos 1–4 and Extended Data Fig. 2a). Similar results were obtained in HCT-8 human colon epithelial cells (Extended Data Fig. 2b,c). Consistent with an effect on spreading, *Salmonella* infection was not affected by these miRNAs (Fig. 2a and Supplementary Table 1).

To move within infected cells and spread to neighbouring cells, *Shigella* relies on actin tails formed by dynamic actin polymerization, which provides the propulsive force for motility[19]. MiR-3668, miR-4732-5p and miR-6073 markedly reduced actin tail formation on *Shigella* infection (Fig. 3b,d). Surprisingly, spreading of *Listeria monocytogenes*, which also exploits actin-based motility[20], remained essentially unaffected by the three miRNAs (Extended Data Fig. 2d).

Together, these results demonstrate that miR-3668, miR-4732-5p and miR-6073 strongly inhibit *Shigella* spreading by preventing actin tail formation.

miRNA-mediated inhibition of *Shigella* actin-based motility is achieved by coordinated targeting of N-WASP. Using bioinformatics prediction tools, specifically TargetScan[21], we identified the neural Wiskott–Aldrich syndrome protein (N-WASP, encoded by the *WASL* gene) as a putative target of the three miRNAs inhibiting *Shigella* spreading. Notably, miR-3668, miR-4732-5p and miR-6073 do not share a common seed sequence (Extended Data Fig. 2e), implying targeting at distinct binding sites. N-WASP is essential for *Shigella* actin-based motility and spreading; it is recruited and activated by the bacterial protein IcsA, and subsequently promotes Arp2/3 complex-mediated actin polymerization[22,23]. Conversely, *Listeria* spreading is independent of N-WASP; it is triggered by the bacterial surface protein ActA, which replaces N-WASP in stimulating actin polymerization[24]. However, N-WASP depletion inhibits bacterial invasion of HeLa cells[25].

In the face of these considerations, the effects of miR-3668, miR-4732-5p and miR-6073 in *Shigella* and *Listeria* infection are consistent with targeting of N-WASP. Accordingly, N-WASP levels were significantly decreased by the three miRNAs (Fig. 3e,f and Extended Data Fig. 2f). Transfection of cells with miR-3668, miR-4732-5p or miR-6073 phenocopies the effects of N-WASP knockdown on *Shigella* and *Listeria* infection (Extended Data Fig. 2g–k). The specificity of N-WASP knockdown and its relevance to infection were further demonstrated by phenotypic rescue experiments using cells expressing short interfering RNA (siRNA)-resistant N-WASP

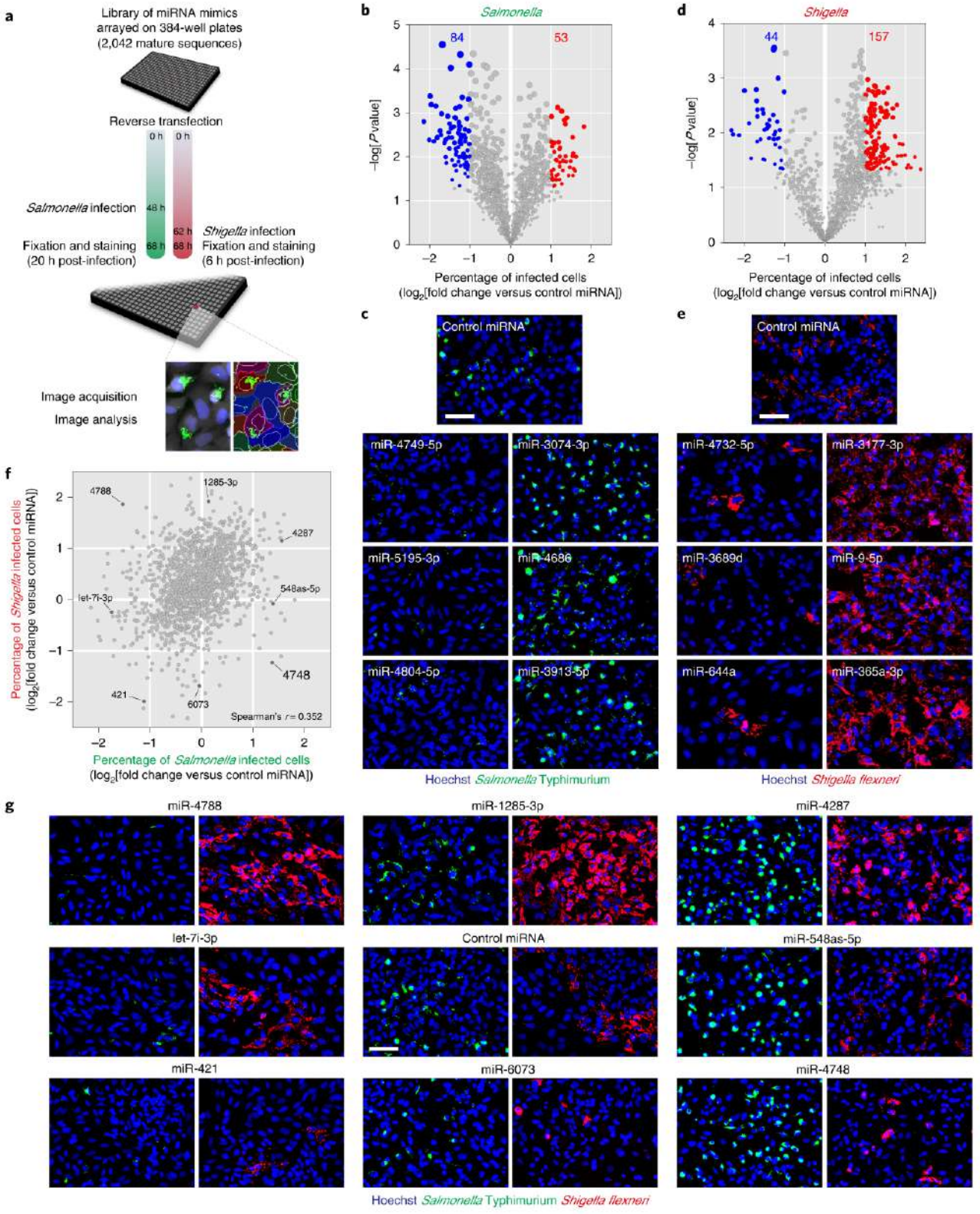

Fig. 1 | Infection by *Salmonella* and *Shigella* are controlled by largely non-overlapping subsets of microRNAs. a, Schematic representation of the screening workflows used to identify miRNAs that regulate *Salmonella* and *Shigella* infection. **b**,**d**, Volcano plot of the effect of human miRNA mimics on the percentage of *Salmonella* (**b**) or *Shigella* (**d**) infected cells, expressed as $\log_2$[fold change] compared with control miRNA. miRNAs highlighted in blue and red significantly decrease or increase infection by at least twofold, respectively ($P < 0.05$; statistical analyses are detailed in Supplementary Table 4). Three independent runs of each screening were performed. **c**,**e**, Representative images of *Salmonella* (**c**) or *Shigella* (**e**) infection in cells transfected with control miRNA or with the top three miRNAs that decrease or increase infection. Data are representative of $n = 3$ biologically independent experiments. Scale bars, 100 µm. **f**, Comparison of the effect of miRNAs on the infection by *Salmonella* and *Shigella*. Results shown are the mean of $n = 3$ independent runs of each screening (**b**,**d**). Spearman's rank correlation coefficient is shown in the bottom right corner. Highlighted miRNAs are shown in **g**. **g**, Representative images of the distinct paradigms of regulation of *Salmonella* and *Shigella* infection by miRNAs. Data are representative of $n = 3$ biologically independent experiments. Scale bar, 100 µm.

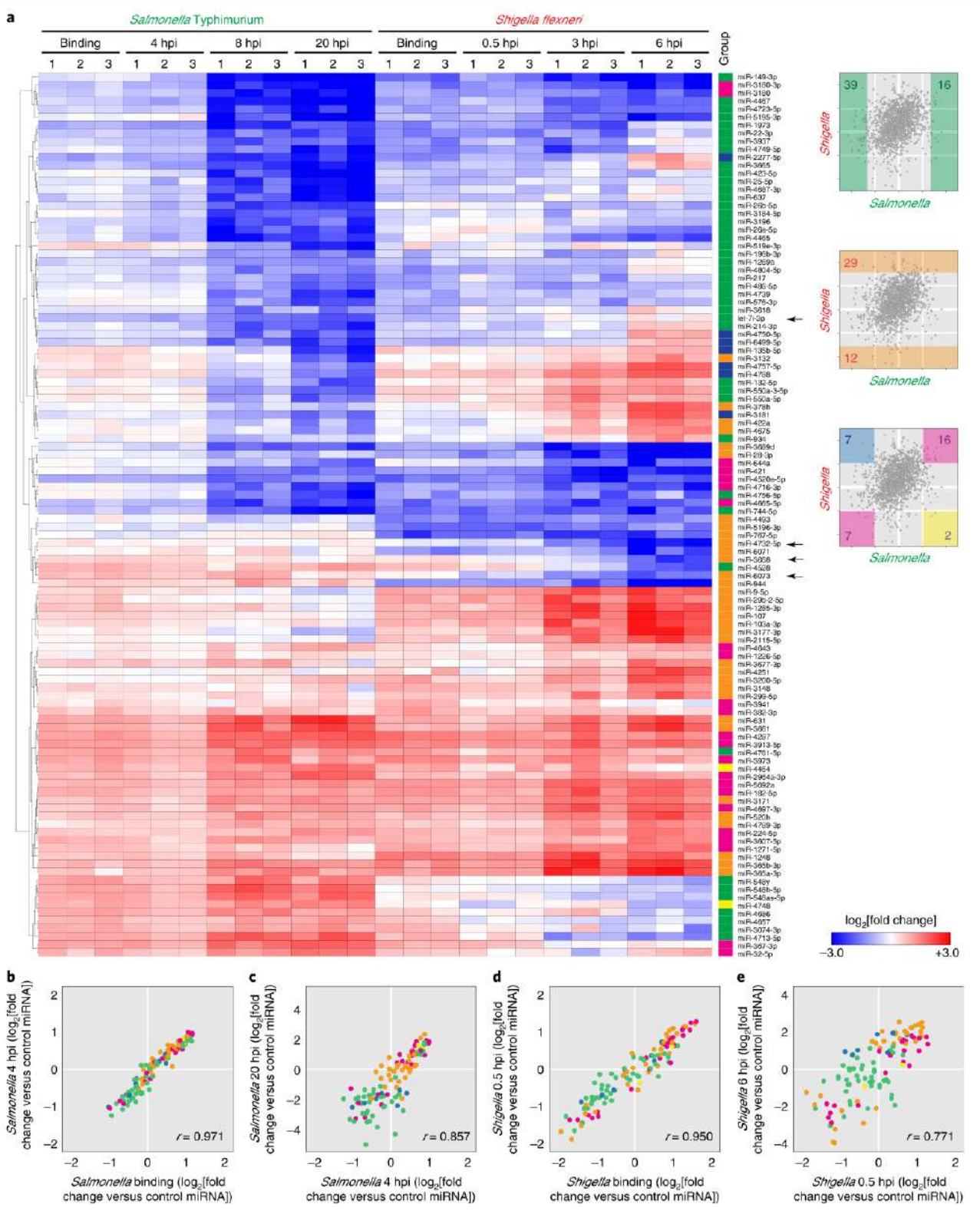

Fig. 2 | miRNAs regulate different stages of *Salmonella* and *Shigella* infection cycles. a. Heat map showing the effect of 110 selected miRNAs on different stages of the infection cycle of *Salmonella* and *Shigella* (binding, early, intermediate and late times post-infection). For each time point, results from $n=3$ biologically independent experiments are shown. Right: plots (similar to Fig. 1f) illustrate the different categories of miRNAs selected for the detailed time-course analysis. Green (55 miRNAs), ≥2.5-fold *Salmonella* infection; orange (41 miRNAS), ≥3-fold *Shigella* infection; pink (23 miRNAs), ≥2-fold infection of both bacteria; blue and yellow (9 miRNAs), opposite effects on the two bacteria (≥2-fold). Hierarchical clustering of the miRNAs was performed based on Euclidean distances. Results are expressed as $\log_2$[fold change] compared with control miRNA. Arrows point to the miRNAs characterized in this study. **b**–**e**, Comparison of the effect of the selected miRNAs on different stages of *Salmonella* (**b**,**c**) and *Shigella* (**d**,**e**) infection. Effects of the miRNAs on binding versus early times post-infection (**b**,**d**) and on early versus late times post-infection (**c**,**e**) are shown. Colours in **b**–**e** correspond to the different miRNA categories identified in **a**. For each time point, results presented are the mean of $n=3$ biologically independent experiments. Spearman's rank correlation coefficients are shown in the bottom right corner of graphs.

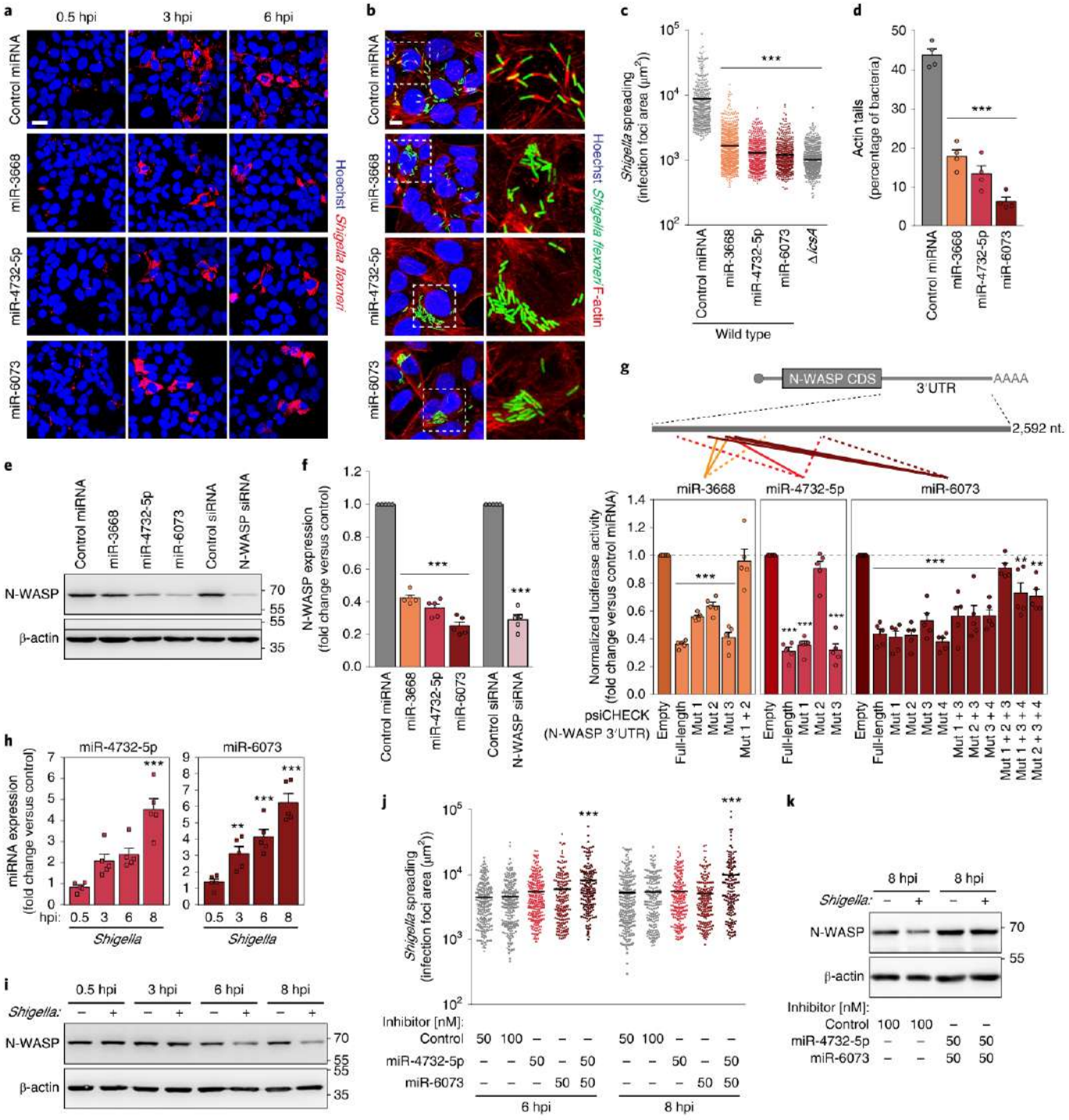

Fig. 3 | *Shigella* actin-based motility and intercellular spreading are inhibited by miR-3668, miR-4732-5p and miR-6073. a,**c**, Representative images (**a**) and area of *Shigella* infection foci (**c**) in HeLa cells transfected with control miRNA, miR-3668, miR-4732-5p or miR-6073 mimics and infected with *Shigella*. Area of infection foci was analysed at 3 hpi; *Shigella* Δ*icsA* mutant (defective in spreading) is shown for comparison. **b**,**d**, Representative images (**b**) and percentage of bacteria forming actin tails (**d**) in HeLa cells transfected with the indicated miRNAs, analysed at 1.5 hpi. Staining of F-actin allows the visualization of actin tails. **e**,**f**, N-WASP expression, determined by western blot (**e**) or quantitative PCR with reverse transcription (RT–qPCR) (**f**), in HeLa cells transfected with the indicated miRNAs or siRNAs. **g**, Schematic representation of the N-WASP 3′UTR; solid lines indicate active miRNA-binding sites; dashed lines point to non-validated putative binding sites. Luciferase activity in cells treated with the miR-3668, miR-4732-5p or miR-6073 mimics is shown compared with cells treated with control miRNA. CDS, coding sequence. **h**, Expression of mature miR-4732-5p or miR-6073, determined by RT–qPCR, in HeLa cells infected with *Shigella*, analysed at different times post-infection. **i**, N-WASP levels, determined by western blot, in HeLa cells mock-treated or infected with *Shigella*. **j**, Area of *Shigella* infection foci in HeLa cells transfected with control miRNA inhibitor or inhibitors of miR-4732-5p, miR-6073 or their combination. **k**, N-WASP levels, determined by western blot, in HeLa cells transfected with control miRNA inhibitor or a combination of miR-4732-5p and miR-6073 inhibitors, and mock-treated or infected with *Shigella*. *Shigella* infection was performed at a multiplicity of infection (MOI) of 25 (**a**,**b**,**d**), 10 (**c**), 100 (**h**,**i**,**k**) or 2.5 (**j**); *Listeria* infection was performed at MOI 20. Scale bars, 25 μm (**a**) and 10 μm (**b**). Results are shown as mean ± s.e.m. of $n = 5$ (**c**,**f**–**h**,**j**) or $n = 4$ (**d**) biologically independent experiments; microscopy images and western blots are representative of $n = 5$ (**a**,**e**,**i**), $n = 4$ (**b**) or $n = 3$ (**k**) biologically independent experiments; centre values indicate the mean (**c**,**j**). $^{**}P < 0.01$ and $^{***}P < 0.001$ (statistical analyses are detailed in Supplementary Table 4).

(EGFP–N-WASPr); additionally, four independent siRNAs targeting N-WASP resulted in a consistent phenotype (Extended Data Fig. 3a–d).

Direct targeting of N-WASP by the three miRNAs was confirmed by 3′ untranslated region (UTR) luciferase reporter assays, and a total of six functional binding sites were identified (miR-3668, two sites; miR-4732-5p, one site; miR-6073, three sites; Fig. 3g and Extended Data Fig. 3e).

Adding to the significance of these findings, expression of endogenous miR-4732-5p and miR-6073 increased in a time-dependent manner during *Shigella* infection (Fig. 3h); miR-3668 was not detected in HeLa or colon epithelial cells (HCT-8, HT-29 and Caco-2). Inversely correlating with the increase of miR-4732-5p and miR-6073, N-WASP expression decreased in *Shigella* infected cells at 6 and 8 hpi (Fig. 3i and Extended Data Fig. 3f).

The use of inhibitors of miR-4732-5p and miR-6073 expression further demonstrated the relevance of these miRNAs for *Shigella* spreading. Whereas inhibition of miR-4732-5p or miR-6073 separately did not change the area of infection foci, simultaneous inhibition of the two miRNAs led to an increase in the area of *Shigella* infection foci, at both 6 and 8 hpi (~180% of control; Fig. 3j). The efficiency of miRNA inhibitors was confirmed (Extended Data Fig. 3g). Notably, blocking the increase of miR-4732-5p and miR-6073 induced by *Shigella* infection completely abrogated N-WASP regulation (Fig. 3k and Extended Data Fig. 3h).

These results reveal an uncharacterized mechanism of host cell defence against *Shigella*, whereby the coordinated up-regulation of miR-4732-5p and miR-6073 expression upon infection results in decreased N-WASP expression, thus preventing bacterial spreading.

Let-7i-3p inhibits *Salmonella* binding and intracellular replication. Among the strongest inhibitors of *Salmonella* infection, we focused on let-7i-3p. This miRNA does not belong to the well-characterized let-7 miRNA family and it has a unique seed sequence; indeed, let-7i-3p is the mature miRNA derived from the -3p arm of the let-7i precursor hairpin (Extended Data Fig. 4a).

In agreement with the time-course studies (Fig. 2a), let-7i-3p inhibition of *Salmonella* infection was already evident at 1 hpi (2-fold) and was even more pronounced at 20 hpi (6.2-fold) (Fig. 4a,b).

To dissect the inhibitory role of let-7i-3p, we performed binding experiments, which revealed a significant decrease of bacteria associated with host cells transfected with let-7i-3p mimic (Fig. 4c,d). This was confirmed using the *Salmonella* Δ4 mutant strain, which binds efficiently to host cells, but is incapable of triggering membrane ruffling and invasion due to the lack of four key effector proteins (SipA, SopE, SopE2 and SopB)[26–28]. The effect of let-7i-3p on *Salmonella* Δ4 binding was similar to its effect on the wild-type strain (Fig. 4c,d), demonstrating that the inhibitory role of let-7i-3p at early stages of infection occurs at the level of *Salmonella* binding to host cells rather than invasion.

Of note, cells transfected with let-7i-3p mimic exhibited a strong increase in actin stress fibres (Fig. 4e). Corroborating these observations, the ratio of filamentous, polymerized actin (F-actin) to globular, monomeric actin (G-actin) was significantly increased by let-7i-3p (Fig. 4f). Treatment with cytochalasin D (an inhibitor of actin polymerization) reversed the inhibitory effect of let-7i-3p on *Salmonella* binding (Extended Data Fig. 4b,c). These results indicate that the actin stress fibres induced by let-7i-3p are responsible for inhibition of *Salmonella* binding.

Similarly to *Salmonella*, *Shigella* binding to host cells was inhibited by let-7i-3p (Fig. 4g and Extended Data Fig. 4d). This was observed for both wild-type *Shigella* and the Δ*ipaB* mutant, which binds efficiently but is unable to invade host cells[29]. The nonspecific electrostatic binding of polylysine (PL)-coated *Salmonella* or *Shigella* to host cells was not inhibited by let-7i-3p (Extended Data Fig. 4e–h).

The inhibitory effect of let-7i-3p on *Salmonella* binding and internalization (1 hpi, 2-fold) cannot itself explain the decrease in number of colony-forming units (cfu) at late times post-infection (8 and 20 hpi, 3.7- and 6.2-fold) (Fig. 4b). This strongly indicates an additional effect of let-7i-3p on *Salmonella* intracellular replication. This was reinforced by quantifying the number of bacteria in individual infected cells at 20 hpi, which showed a 3-fold decrease following treatment with the let-7i-3p mimic (Fig. 4h,i). Although the early steps of *Shigella* infection were also inhibited by let-7i-3p (binding at 0.5 hpi; Figs. 2a and 4g,j,k and Extended Data Fig. 4d), this effect was lost at late infection times (6 hpi; Figs. 2a and 4j,k). *Listeria* binding and intracellular replication were not affected by let-7i-3p (Extended Data Fig. 4i–l).

Overall, these results demonstrate that let-7i-3p acts on two distinct steps of *Salmonella* infection, inhibiting both the bacterial binding and intracellular replication.

Let-7i-3p inhibits *Salmonella* intracellular replication via targeting of RGS2. Considering its strong effect on *Salmonella* infection, we reasoned that let-7i-3p expression could be modulated during infection. Indeed, let-7i-3p expression decreases upon *Salmonella* infection, in a MOI- and time-dependent manner (Fig. 5a,b). Of note, infection with the *Salmonella* ΔSPI-2 strain (defective in intracellular replication) also reduced let-7i-3p, whereas infection with the ΔSPI-1 strain (defective in invasion) had no effect on let-7i-3p (Fig. 5a). Overall, these results indicate that *Salmonella* counteracts let-7i-3p inhibitory effect by decreasing its expression.

To obtain a comprehensive overview of let-7i-3p targets, we performed a comparative transcriptomic analysis of cells transfected with let-7i-3p or control miRNA mimics. This analysis revealed 1,620 genes that were downregulated by let-7i-3p (more than 1.5-fold; Fig. 5c). Additionally, we assessed transcriptome changes elicited by *Salmonella* infection (20 hpi, MOI 100); 545 genes were upregulated upon *Salmonella* infection (more than 2-fold; Fig. 5c). Considering that let-7i-3p expression decreases upon *Salmonella* infection (Fig. 5a,b), a subset of the genes upregulated during infection presumably corresponds to de-repressed let-7i-3p targets. Thus, by comparing genes downregulated by let-7i-3p with those upregulated by *Salmonella* infection, we identified 23 targets potentially relevant for *Salmonella* infection ($P < 2.4 \times 10^{-4}$; Fig. 5c).

We focused our attention on RGS2 (regulator of G-protein signalling 2), a GTPase-activating protein for heterotrimeric G-protein α-subunits[30]. RGS2 has also been shown to have G-protein-independent functions, including modulation of protein synthesis, microtubule polymerization and ion channels[31]. Although RGS2 is strongly upregulated upon *Salmonella* infection (Fig. 5d–g), its role on infection has not been previously addressed. Consistent with RGS2 being a bona fide target of let-7i-3p, its expression inversely correlated with let-7i-3p levels (compare Fig. 5d–g and 5a,b) and the increase of RGS2 upon infection was dependent on bacterial internalization (Fig. 5d,f). A decrease in RGS2 subsequent to let-7i-3p mimic transfection was also confirmed (Fig. 5h,i).

Additionally, we determined that let-7i-3p expression is not altered upon *Shigella* or *Listeria* infection (Extended Data Fig. 4m,n), and that RGS2 expression is not changed upon *Listeria* infection, although it increases slightly in *Shigella* infected cells (1.8-fold at 6 hpi; Extended Data Fig. 4o,p). It should be noted that this increase in RGS2 is significantly smaller than that observed for *Salmonella* (approximately eightfold; Fig. 5d,e). These results demonstrate that the strong regulation of let-7i-3p and, conversely, of RGS2 expression, is not a general response to bacterial infection, but is restricted to *Salmonella* infection.

Reporter assays showed that let-7i-3p targets the RGS2 coding sequence, rather than its 3′UTR. We identified three non-overlapping regions regulated by let-7i-3p and pinpointed one binding site in fragment F1 (Extended Data Fig. 5a–e).

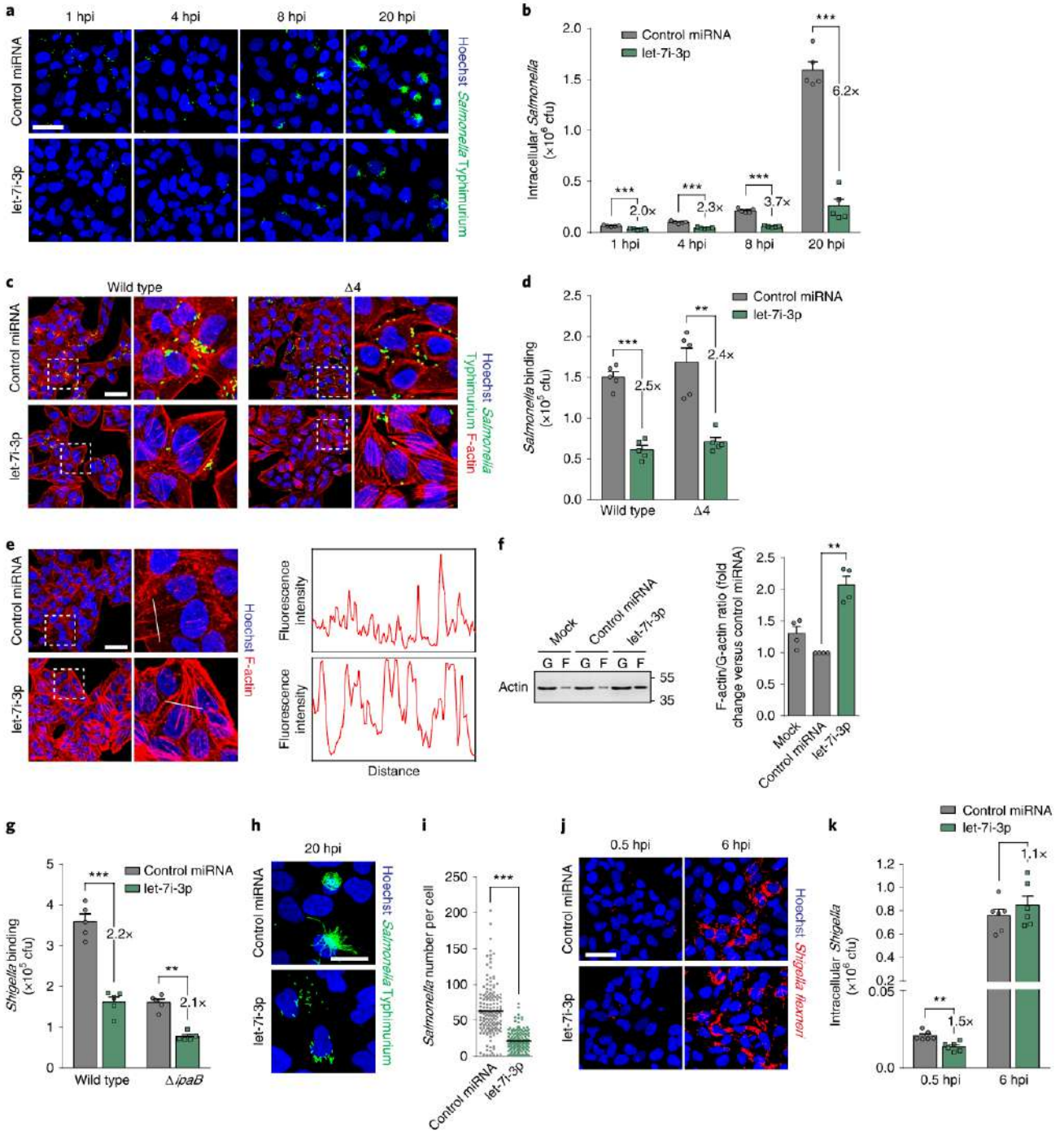

Fig. 4 | Let-7i-3p inhibits *Salmonella* binding to host cells and bacterial intracellular replication. a,**b**, Representative images (**a**) and quantification of intracellular *Salmonella* by cfu (**b**) of HeLa cells infected with *Salmonella* following transfection with control miRNA or let-7i-3p mimics and analysed at the indicated times post-infection. **c**,**d**, Representative images (**c**) and quantification by cfu (**d**) of *Salmonella* bound to HeLa cells transfected with control miRNA or let-7i-3p mimics, incubated with *Salmonella* wild-type or Δ4 strain (binding proficient and invasion deficient) for 10 min. **e**, Representative images of F-actin staining of HeLa cells transfected with control miRNA or let-7i-3p mimics. Graphs show fluorescence intensity of the phalloidin staining measured along the indicated lines. **f**, F-actin and G-actin content of HeLa cells transfected with control miRNA or let-7i-3p mimics, or mock-transfected; F-actin:G-actin ratios were calculated on the basis of the quantification of the western blots. **g**, Quantification by cfu of *Shigella* bound to HeLa cells transfected with control miRNA or let-7i-3p mimics and incubated with *Shigella* wild-type or Δ*ipaB* mutant strain (binding proficient and invasion deficient) for 25 min. **h**,**i**, Representative confocal microscopy images (**h**) and number of *Salmonella* per cell (**i**) of HeLa cells transfected with control miRNA or let-7i-3p mimics, infected with *Salmonella* and analysed at 20 hpi. Combined data for 163 (control miRNA) or 156 (let-7i-3p) infected cells is shown, obtained from $n=3$ biologically independent experiments (centre values indicate mean). **j**,**k**, Representative images (**j**) and quantification of intracellular *Shigella* by cfu (**k**) of HeLa cells transfected with control miRNA or let-7i-3p mimics. *Salmonella* infection was performed at MOI 25 (**a**,**b**,**h**,**i**) or MOI 50 (**c**,**d**). *Shigella* infection was performed at MOI 25 (**j**,**k**) or MOI 50 (**g**). Scale bars, 50 µm (**a**,**c**,**e**,**j**) and 25 µm (**h**). Results are shown as mean ± s.e.m. of $n=4$ (**f**), $n=5$ (**b**,**d**,**g**) or $n=6$ (**k**) biologically independent experiments; microscopy images are representative of $n=5$ (**a**,**c**,**j**) or $n=4$ (**e**) biologically independent experiments; $^{**}P<0.01$ and $^{***}P<0.001$ (statistical analyses are detailed in Supplementary Table 4).

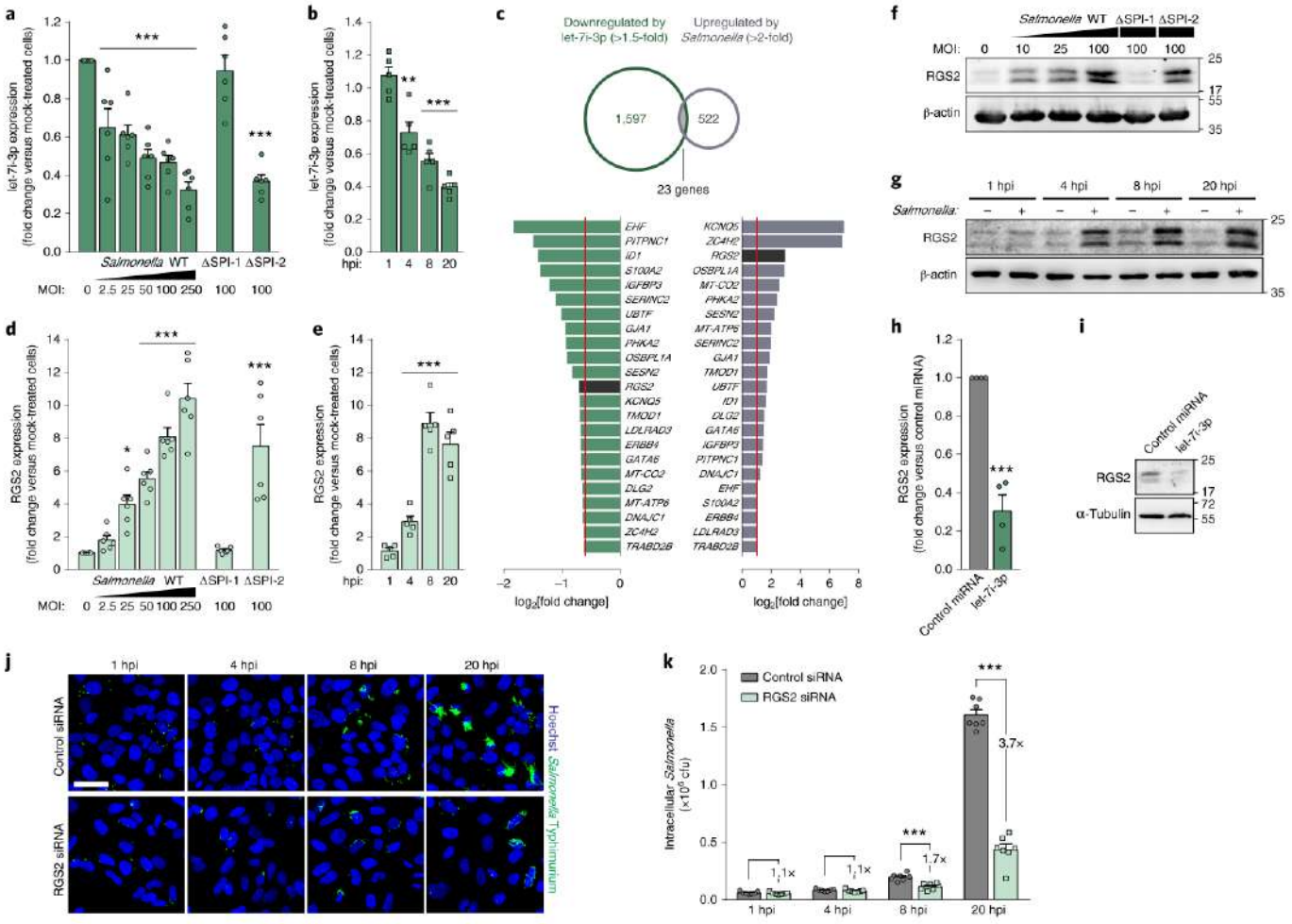

Fig. 5 | Inhibition of *Salmonella* replication by let-7i-3p is mediated by RGS2. a,b, Expression of mature let-7i-3p, evaluated by RT-qPCR, in HeLa cells infected with wild-type (WT) *Salmonella* at increasing MOI (2.5–250), or ΔSPI-1 (invasion defective) or ΔSPI-2 (defective in intracellular replication) mutant strains at MOI 100, analysed at 20 hpi (**a**), or infected with wild-type *Salmonella* at MOI 100 and analysed at 1, 4, 8 and 20 hpi (**b**). **c**, Overlap between genes downregulated by let-7i-3p overexpression (>1.5-fold) and genes upregulated upon *Salmonella* infection (>2-fold; MOI 100; 20 hpi). Expression changes of the 23 overlapping genes are shown (fold change relative to control miRNA or mock-treated cells); red lines indicate 1.5- and 2-fold thresholds. **d,e**, Expression of mature RGS2, evaluated by RT-qPCR, in HeLa cells infected with wild-type *Salmonella* at increasing MOI (2.5–250), or with ΔSPI-1 or ΔSPI-2 mutant strains at MOI 100, analysed at 20 hpi (**d**), or infected with wild-type *Salmonella* at MOI 100 and analysed at 1, 4, 8 and 20 hpi (**e**). **f,g**, RGS2 protein levels, determined by western blot, in HeLa cells infected with wild-type *Salmonella* at increasing MOI (10–100), or ΔSPI-1 or ΔSPI-2 mutant strains (MOI 100), and analysed at 20 hpi (**f**), or infected with wild-type *Salmonella* (MOI 100) and analysed at 1, 4, 8 and 20 hpi (**g**). **h,i**, RGS2 expression, determined by RT-qPCR (**h**) or western blot (**i**), in HeLa cells transfected with control miRNA or let-7i-3p mimics. **j,k**, Representative images (**j**) and quantification of intracellular *Salmonella* by cfu (**k**) of HeLa cells transfected with control siRNA or RGS2 siRNA. Infection was performed at MOI 25 and analysed at 1, 4, 8 and 20 hpi. Scale bar, 50 µm. Results are shown as mean ± s.e.m. of $n=4$ (**h**), $n=5$ (**b**,**e**), $n=6$ (**a**,**d**) or $n=7$ (**k**) biologically independent experiments; western blots and microscopy images are representative of $n=5$ (**f**,**g**,**j**) or $n=3$ (**i**) biologically independent experiments. $^{*}P<0.05$, $^{**}P<0.01$ and $^{***}P<0.001$ (statistical analyses are detailed in Supplementary Table 4).

RGS2 knockdown had no effect on *Salmonella* infection at early times (1 and 4 hpi), but strongly impaired infection at intermediate and late times after infection (8 and 20 hpi; Fig. 5j,k). Efficient knockdown of RGS2 was confirmed (Extended Data Fig. 5f). The specificity of RGS2 knockdown was further demonstrated by phenotypic rescue experiments in cells expressing a siRNA-resistant RGS2 (EGFP–RGS2r); moreover, four independent siRNAs targeting RGS2 reduced *Salmonella* replication (Extended Data Fig. 5g–j).

These results indicate that the decrease of let-7i-3p expression upon *Salmonella* infection increases RGS2 levels, which are required to sustain productive *Salmonella* intracellular replication.

Targeting of RGS2 by let-7i-3p increases lysosomal degradative function. As let-7i-3p impairs *Salmonella* intracellular replication while not affecting *Shigella*, we hypothesized that its action could affect the vacuolar intracellular lifestyle of *Salmonella*[17,32]. SCVs are characterized by an acidic environment and the presence of late endosomal and lysosomal markers (for example LAMP-1); mannose-6-phosphate receptors (MPRs) and lysosomal hydrolytic enzymes do not accumulate in these compartments[33–37].

Transfection with let-7i-3p miRNA mimic or RGS2 siRNA resulted in an abnormally high accumulation of acidic vesicles (labelled with Lysotracker; Fig. 6a) and vesicles positive for LAMP-1 (Fig. 6b). Moreover, increased labelling of vesicles with DQ Red–BSA was observed, indicating higher lysosomal proteases activity (Fig. 6c). Treatment of transfected cells with wortmannin or amiodarone, drugs that redistribute MPRs leading to mistargeting of lysosomal enzymes[38–42], reduced the accumulation of DQ

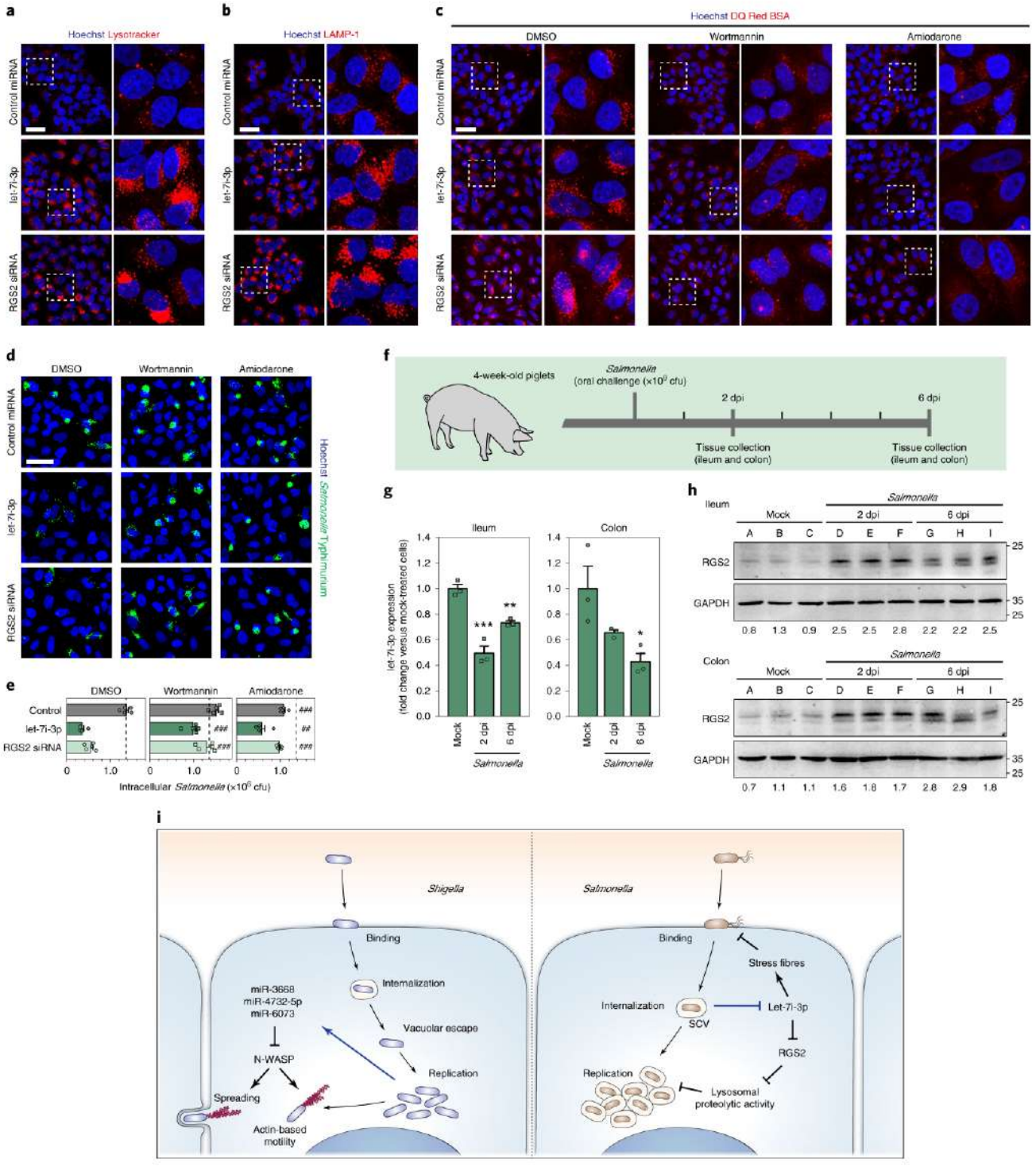

Fig. 6 | Modulation of endolysosomal trafficking by let-7i-3p is critical for *Salmonella* infection. a–c, Representative images of HeLa cells transfected with control miRNA, let-7i-3p mimics or RGS2 siRNA and stained with Lysotracker (**a**), for LAMP-1 (**b**), or with DQ Red-BSA following treatment with DMSO, wortmannin or amiodarone (**c**). Images are representative of $n=3$ biologically independent experiments. Scale bars, 50 µm. **d,e**, Representative images (**d**) and quantification of intracellular *Salmonella* by cfu (**e**) in HeLa cells transfected with control miRNA, let-7i-3p mimics or RGS2 siRNA and treated with DMSO, wortmannin or amiodarone and analysed at 20 hpi. Infection was performed at MOI 25. Data are representative (**d**) or shown as mean ± s.e.m. (**e**) of $n=5$ biologically independent experiments; $^{\#\#}P<0.01$ and $^{\#\#\#}P<0.001$ relative to DMSO (statistical analyses are detailed in Supplementary Table 4). Scale bar, 50 µm. **f**, Schematic representation of in vivo *Salmonella* infection experiments. **g,h**, Expression of mature let-7i-3p, evaluated by RT-qPCR (**g**) and of RGS2 evaluated by western blot (**h**) in ileum and colon samples obtained from untreated piglets (mock) or piglets challenged with *Salmonella*, at 2 and 6 d post-infection (dpi). Three animals were analysed per condition per time point. Values below western blots indicate RGS2:GAPDH ratios; averages of the three control samples were set to 1. Results are shown as mean ± s.e.m.; $^{*}P<0.05$, $^{**}P<0.01$ and $^{***}P<0.001$ (statistical analyses are detailed in Supplementary Table 4). **i**, Model depicting the selective effects of miRNAs on the life cycle of *Shigella* and *Salmonella*. MiR-3668, miR-4732-5p and miR-6073, through targeting of N-WASP, restrict *Shigella* infection by inhibiting *Shigella* actin-based motility and intercellular spreading; let-7i-3p, by its target RGS2, alters endolysosomal trafficking and vacuolar environment, ultimately modulating *Salmonella* intracellular replication.

Red-BSA-positive vesicles (Fig. 6c) and, importantly, antagonized the inhibitory effect of let-7i-3p overexpression and RGS2 knockdown on *Salmonella* replication (Fig. 6d,e). Although wortmannin was shown to induce *Salmonella* vacuolar escape and cytoplasmic replication[43], in our experiments the treatment was started at 7 hpi and no increase of cells with hyper-replicating bacteria was observed (Fig. 6d).

These results demonstrate that let-7i-3p and its target RGS2 regulate *Salmonella* replication through modulation of the endolysosomal trafficking network.

Decrease of let-7i-3p expression sustains in vitro and in vivo *Salmonella* infection. The biological relevance of let-7i-3p down-regulation during infection was further explored using a specific miRNA inhibitor. Inhibition of let-7i-3p significantly favoured infection (Extended Data Fig. 6a,c). As expected, RGS2 expression was de-repressed as a consequence of let-7i-3p inhibition, and a decrease in LAMP-1-positive, Lysotracker- and DQ Red–BSA-labelled vesicles was observed (Extended Data Fig. 6b,d–f).

Having shown that changes of let-7i-3p and RGS2 during *Salmonella* infection have a prominent effect on the outcome of infection in vitro, we next examined whether this could be observed in vivo, opting for a piglet model of *Salmonella* infection[44]. Analysis of let-7i-3p expression in ileum and colon tissue samples of control (mock) or *Salmonella*-infected animals, collected at 2 and 6 dpi showed reduced levels of let-7i-3p (Fig. 6f,g). Conversely, and in perfect agreement with the in vitro data, RGS2 expression was significantly increased (Fig. 6f,h). Of note, let-7i-3p sequences are identical in pig and human.

Taken together, these observations demonstrate that let-7i-3p is critical to the outcome of *Salmonella* infection and that, by decreasing let-7i-3p expression, *Salmonella* relieves the inhibition posed by this miRNA on two distinct steps of its infection cycle.

Discussion

We report a systematic genome-wide screening approach to identify miRNAs that regulate infection by two relevant bacterial pathogens—*Salmonella* and *Shigella*. A significant fraction of miRNAs (about 15%, 317 out of 2,042 using a twofold threshold; $P<0.05$) modulated infection by at least one of the pathogens, impinging on different stages of the bacterial infection cycle.

The comparative analysis of these datasets was particularly interesting, revealing a small overlap between the subsets of miRNAs affecting *Salmonella* and *Shigella* infection. This most probably reflects the disparate intracellular lifestyles of the two bacterial pathogens and potentially highlights specific intracellular requirements for infection. By this reasoning, miRNAs exhibiting a selective action on *Shigella* infection would be expected to affect host cell functions related to cytosolic replication or actin-based motility, whereas miRNAs with selective effects on *Salmonella* infection are likely to target intracellular processes relevant to SCV formation, maturation and stability. This is exemplified by miR-3668, miR-4732-5p and miR-6073, which specifically inhibit *Shigella* infection, and let-7i-3p, a strong inhibitor of *Salmonella* infection. Indeed, miR-3668, miR-4732-5p and miR-6073, by targeting N-WASP, inhibit *Shigella* actin-based motility and intercellular spreading, restricting *Shigella* infection (Fig. 6i). Let-7i-3p acts through modulation of endolysosomal trafficking, via RGS2, modifying the vacuolar environment and, thus, inhibiting *Salmonella* intracellular replication (Fig. 6i).

During the last decade, miRNAs have been increasingly recognized as having key roles in the host–pathogen interface[4,5]. The two cases explored here illustrate two paradigms of miRNA modulation in the context of infection, working either as part of the host defence (miR-4732-5p/miR-6073 and *Shigella*) or favouring bacterial pathogenesis (let-7i-3p and *Salmonella*).

While the pivotal role of N-WASP in actin tail formation, intracellular motility and intercellular spreading of *Shigella* is well characterized[22,23], regulation of N-WASP during infection has not been reported previously. Considering the strong up-regulation of miR-4732-5p and miR-6073 and the consequent down-regulation of N-WASP, we argue that the convergent up-regulation of these two miRNAs is a host defence strategy aimed at preventing *Shigella* spreading.

An aspect of particular relevance is that, among the strongest inhibitors of *Shigella* infection, we found three miRNAs that compromise *Shigella* spreading to neighbouring cells, all acting through direct regulation of N-WASP. Given that different miRNAs can act cooperatively to more efficiently repress targets[45,46], our results reveal the relevance of miRNA-dependent N-WASP regulation, with potential implications for other biological processes dependent on N-WASP[47]. It has also been shown that multiple binding sites for the same miRNA can substantially increase target repression[45,46]. We identified six functional binding sites for the three miRNAs, reinforcing the functional relevance of N-WASP targeting by miRNAs.

Furthermore, we identified the let-7i-3p miRNA that acts on two distinct steps of *Salmonella* infection: binding and intracellular replication. This dual effect appears to be a recurrent feature among miRNAs with strong impact on infection. Along these lines, we recently demonstrated that miR-29b-2-5p, one of the top miRNAs increasing *Shigella* infection, promotes bacterial capture by host cells by increasing filopodia formation and, in addition, it increases intracellular replication[48].

Given that actin cytoskeleton reorganization is a hallmark of *Salmonella* and *Shigella* entry sites, in which both bacterial and host factors participate[49,50], we hypothesized that the stress fibres induced by let-7i-3p could be detrimental for infection. This is supported by the observation that treatment of cells overexpressing let-7i-3p with cytochalasin D, or nonspecific binding of polylysine-coated bacteria, overcomes the inhibitory effect of let-7i-3p on bacterial binding. Overall, our results support a model in which the actin stress fibres induced by let-7i-3p modify cellular parameters (for example cell shape, membrane stiffness or composition, cell–cell contacts) that influence binding of *Salmonella* or *Shigella* to host cells. It is conceivable that the lack of effect of let-7i-3p on *Listeria* binding is linked to the different entry mechanisms (zipper versus trigger), and therefore different host requirements.

The observation that the inhibitory effect of let-7i-3p on intracellular *Salmonella* replication could be reversed by interfering with MPR-mediated targeting of lysosomal enzymes indicates that the role of let-7i-3p and its target RGS2 on lysosomal function is the major determinant of their impact on *Salmonella* replication. Of note, before the present study neither let-7i-3p nor RGS2 had been implicated in the modulation of endolysosomal trafficking. However, it has been suggested that RGS proteins could be targeted to intracellular organelle membranes due to their interaction with Gα subunits and thus be involved in the regulation of secretory trafficking[51]. Our study reveals a mechanism by which *Salmonella* modulates lysosomal function: by down-regulating let-7i-3p, *Salmonella* infection de-represses RGS2 expression, consequently blunting lysosomal activity, ultimately favoring bacterial intracellular replication. We propose that this mechanism works concomitantly to that described by McGourty et al., involving misrouting of lysosomal enzymes through the formation of a complex containing the bacterial effector protein SifA and the host proteins (SKIP and Rab9), leading to sequestration of Rab9 in SCVs, and compromising retrograde transport of MPRs[52].

Although RNA sequencing has undoubtedly revealed host miRNome changes as a hallmark of infection by bacterial pathogens, the functional relevance of the majority of these regulations is still elusive. Here, we show that the application of systematic approaches to study miRNA function, namely phenotypic

screenings, can uncover a wealth of insightful information. Finally, the datasets from this comprehensive large-scale study constitute a valuable resource for further investigations aimed at uncovering previously unknown molecular players and pathways relevant to host–pathogen crosstalk.

Methods

Mammalian cell culture. Human epithelial HeLa-229 (ATCC, CCL-2.1) were cultured in DMEM GlutaMAX containing 1.0 g l^{-1} glucose (Life Technologies, 21885) and human colon cancer HCT-8 (ATCC, CCL-244) were cultured in RPMI 1640 GlutaMAX (Life Technologies, 72400). Cell lines were acquired from ATCC–LGC Standards and no further authentication was performed. The UNC5C-knockout HeLa-229 cell line (UNC5C KO) was previously described[48]. Media were supplemented with 10% fetal bovine serum (Biochrom, S0115). Cells were maintained at 37 °C in a humidified atmosphere with 5% CO_2. All cell lines tested negative for mycoplasma contamination.

Bacterial strains. *Shigella flexneri* serotype 5 strain M90T wild-type or expressing GFP or mCherry from plasmids[53], *Salmonella enterica* serovar Typhimurium strain SL1344 expressing GFP constitutively from a chromosomal locus[54] and *Listeria monocytogenes* serovar 1/2a EGD-e were used in this study. The *Shigella* Δ*icsA*, *Salmonella* ΔSPI-1 and ΔSPI-2 mutant strains were previously described[48,55]. The *Salmonella* Δ4 strain (Δ*sopB*, Δ*sipA*, Δ*sopE*, Δ*sopE2*) was kindly provided by J. E. Galán (Yale University, USA). For piglet infections, *Salmonella enterica* serovar Typhimurium phagetype DT104 isolated from a carrier pig[56], was used. *Shigella* and *Salmonella* were grown aerobically in Luria broth (LB) medium and *Listeria* was grown in brain heart infusion medium. When appropriate, medium was supplemented with the following antibiotics: ampicillin 100 μg ml^{-1}, chloramphenicol 20 μg ml^{-1} or kanamycin 25 μg ml^{-1}.

Bacterial infections. For *Salmonella* and *Shigella* infections, overnight cultures were diluted 1:100 in LB and grown at 37 °C with shaking until optical density at 600 nm (OD_{600}) was 2 (*Salmonella*) or 0.4 (*Shigella*). Bacteria were then collected by centrifugation for 2 min at 12,000*g* and resuspended in complete medium. Unless otherwise specified, cells were infected with *Salmonella* or *Shigella* at MOI 25. After addition of bacteria, cells were centrifuged at room temperature at 250*g* for 10 min (*Salmonella*) or 2,000*g* for 15 min (*Shigella*) and incubated at 37 °C in a 5% CO_2 humidified atmosphere for 20 min (*Salmonella*) or 15 min (*Shigella*). Extracellular bacteria were killed by replacing medium with fresh medium containing 50 μg ml^{-1} gentamicin for 30 min. Medium was then exchanged to medium containing 10 μg ml^{-1} gentamicin until analysis. For *Listeria* infections, overnight cultures were diluted 1:50 in brain heart infusion medium and grown at 37 °C with shaking until OD_{600} was 0.7. Dilution of bacterial cultures and infections were performed as described above for *Salmonella*.

For binding experiments, cells were exposed to *Salmonella* (MOI 50), *Shigella* (MOI 50) or *Listeria* (MOI 50) as described above, washed thoroughly with PBS and processed immediately after the centrifugation step (*Salmonella*) or after a 10 min incubation at 37 °C (*Shigella* and *Listeria*). When indicated, *Salmonella* and *Shigella* were coated with polylysine before infection. In brief, bacteria were washed with PBS and coated with 10 μg ml^{-1} polylysine (Sigma, 6407) in PBS for 10 min at room temperature.

For *Shigella* actin tail quantification experiments, cells were infected as described above (MOI 10) and analysed at 1.5 hpi. For quantification of *Shigella* and *Listeria* spreading, cells were analysed at 3, 6 or 8 hpi (*Shigella*) or 8 hpi (*Listeria*).

For the quantification of miR-3668, miR-4732-5p and miR-6073 expression and N-WASP protein levels, *Shigella* infection was performed in UNC5C KO cells. As previously described, infection in this cell line is markedly higher than in wild-type HeLa-229 cells[48].

To quantify bacteria binding or intracellular replication by cfu assays, cells were washed three times with PBS and lysed with PBS containing 0.1% Triton-X-100. Cell lysates were serially diluted in PBS and plated on LB plates.

To block actin polymerization, HeLa-229 cells were treated with 0.5 μg ml^{-1} cytochalasin D (Sigma, C8273) for 1 h before infection. To induce secretion of hydrolytic enzymes to the extracellular medium, HeLa-229 cells were treated with 2.5 μM amiodarone (Sigma, A8423) or 100 nM wortmannin (Sigma, W1628) at 7 hpi; treatments were maintained until analysis.

High-throughput miRNA screenings. The genome-wide library of miRNA mimics (miRIDIAN miRNA mimics, CS-001030) corresponding to all human mature miRNAs (2,042 miRNAs, 2,019 unique sequences, miRBase 19.0) was obtained from Dharmacon. The screenings were performed essentially as described previously[8,13]. In brief, miRNAs were transferred, using an automated liquid handling station (Hamilton STAR), from library stock plates to 384-well plates (Viewplate-384 black, clear bottom, PerkinElmer). miRNAs were transfected into HeLa-229 cells by a standard reverse transfection protocol (final miRNA concentration 50 nM) using the transfection reagent Lipofectamine RNAi-MAX (Life Technologies, 13778030); 1.5×10^3 cells were seeded per well. Cells were infected with GFP-labelled *Salmonella* SL1344 or *Shigella* M90T (MOI 25) 48 or 62 h after transfection, respectively, as described above. Cells were fixed at 20 hpi (*Salmonella*) or 6 hpi (*Shigella*) and processed for microscopy analysis. Transfection efficiency was confirmed using a siRNA targeting the essential ubiquitin C gene (*UBC*), resulting in the death of virtually all cells. A *Caenorhabditis elegans* miRNA (cel-miR-231; control miRNA) was used as negative control. Three independent runs were performed for each screening.

For the *Salmonella* screening, cells were stained with HCS CellMask Deep Red stain (1:15,000; Life Technologies, H32721) and Hoechst 33342 (1:5,000; Life Technologies, H3570), according to the manufacturer's instructions. For the *Shigella* screening, cells were stained with a primary antibody directed against *Shigella* lipopolysaccharide (LPS) (1:150, 2 h at room temperature; Gentaur, YCC310-130), followed by secondary antibody conjugated with Alexa Fluor 488 (1:400, 1 h at room temperature; Life Technologies, A21441). Finally, cells were stained with HCS CellMask Deep Red stain and Hoechst 33342 as described for the *Salmonella* screening.

miRNAs that decreased the cell number of host cells to less than 65% of the average of all samples for each individual run of the screenings were considered toxic and excluded from further analysis.

For the validation and time-course experiments using mimics of the 110 selected miRNA, procedures were performed essentially as described for the genome-wide screenings.

miRNA and siRNA transfection. miRNA mimics, miRNA inhibitors and siRNAs were transfected with Lipofectamine RNAi-MAX (Life Technologies, 13778030) using a reverse transfection protocol, as described above for the screenings. HeLa-229 and HCT-8 cells were transfected with miRNA mimics or inhibitors at a final concentration of 50 nM. For RGS2 and N-WASP siRNA transfection, cells were transfected at a final concentration of 25 nM and 12.5 nM, respectively. For confocal microscopy, cfu assays and RNA-isolation experiments, cells were seeded in 24-well plates, at a density of 6.0×10^4 cells per well; for western blot, 2.4×10^5 cells were seeded per well in 6-well plates.

siGENOME non-targeting siRNA #5 (D-001210-05), SMARTpool siGENOME WASL siRNA (M-006444-02), individual siGENOME Human WASL siRNA (D-006444-02, D-006444-03, D-006444-05 and D-006444-06), individual siGENOME Human RGS2 siRNA (D-009887-01, D-009887-02, D-009887-04 and D-009887-05), miRIDIAN microRNA mimic negative control #4 (cel-miR-231; CN-004000-01), miRIDIAN microRNA hsa-let-7i-3p mimic (C-301044-01), hsa-miR-3668 mimic (C-301549-00), hsa-miR-4732-5p mimic (C-302317-00), hsa-miR-6073 mimic (C-302627-00), miRIDIAN microRNA Hairpin Inhibitor Negative Control #4 (IN-004005-01) and miRIDIAN microRNA hsa-let-7i-3p hairpin inhibitor (IH-301044-02) were purchased from Dharmacon. RGS2 (SASI_Hs01_00126554) pre-designed siRNA was purchased from Sigma. Negative control A miRCURY LNA miRNA Inhibitor Control (YI00199006), hsa-miR-4732-5p miRCURY LNA miRNA Inhibitor (YI04106116) and hsa-miR-6073 miRCURY LNA miRNA Inhibitor (YI04104767) were purchased from Qiagen.

siRNA rescue experiments. For the siRNA rescue experiments, HeLa-229 cells stably expressing GFP-tagged N-WASP or RGS2, with either the wild-type protein or the siRNA-resistant mutant (4–5 synonymous mutations in the siRNA-binding region) were generated. Mutants of the siRNA binding site in plasmids EGFP–N-WASP[57] (addgene #47406, gift from P. McPherson) and EGFP–RGS2 (see below) were generated by site directed mutagenesis. Lentiviral transfer plasmids for the generation of stable cell lines were assembled in the pLJM1-EGFP plasmid[58] backbone (addgene #19319, gift from D. Sabatini). In brief, wild-type and siRNA-resistant versions of EGFP–N-WASP were excised with AgeI and EcoRI, and siRNA-resistant versions of EGFP-RGS2 were excised with AgeI and MfeI; both were subcloned in the pLJM1-EGFP plasmid between the AgeI and EcoRI restriction sites. All primers used for cloning and mutagenesis are indicated in Supplementary Table 3.

For each construct, lentiviral particles were produced in HEK293T using the psPAX2 and pMD2.G packaging plasmids (addgene #12260 and #12259, gift from D. Trono) using Lipofectamine 3000 (Life Technologies, L-3000015) according to the manufacturer's instructions. Viral supernatants were collected at 48 h and 72 h after transfection, combined and centrifuged at 350*g*, filtered through a 0.45 μm filter and used immediately for transduction. Lentiviral transduction of HeLa-229 cells was performed using different dilutions of the viral supernatants in 6-well plates containing 4×10^5 cells per well in media supplemented with 8 μg ml^{-1} polybrene (Sigma, H9268). Puromycin selection (400 ng ml^{-1}) was started 24 h after transduction and maintained for additional 72 h. The surviving cell populations were sorted in a FACSAria III cell sorter (BD Biosciences) to enrich for homogenous populations of EGFP-positive cells. Cells transduced at low MOIs were used to minimize multiple integration events.

Parental and stable cell lines were transfected with siRNAs (N-WASP siRNA, Dharmacon individual siGENOME Human WASL siRNA D-006444-02; RGS2 siRNA, Sigma SASI_Hs01_00126554) and infected with *Salmonella* or *Shigella* as described above.

Staining and immunofluorescence. Cells seeded in glass coverslips or 384-well plates (Viewplate-384 black, clear bottom, PerkinElmer) were fixed with 4%

paraformaldehyde for 15 min at room temperature, permeabilized with 0.5% Triton-X-100 in PBS for 10 min, followed by blocking in 1% Bovine Serum Albumin (BSA) in PBS for 30 min; for *Listeria* staining, permeabilization was performed for 30 min. Cells were then stained with the following primary antibodies diluted in blocking solution: rabbit antibody against *Shigella* LPS (1:150, 2 h at room temperature; Gentaur, YCC310-130), rabbit antibody against *Listeria* (1:750, 2 h at room temperature; antibodies-online, ABIN 237765) or mouse monoclonal antibody against LAMP-1 (1:100, overnight at 4 °C; Santa Cruz, sc-20011). Cells were washed with PBS and incubated with the corresponding secondary antibodies conjugated with Alexa Fluor 488 or 594 (1:250, 1 h at room temperature; Life Technologies, A21441, A21442 or A21201).

For F-actin staining, following the blocking step, cells were incubated for 1 h with Alexa Fluor 594 or 488 Phalloidin (1:50; Life Technologies, A12381 and A12379). For staining of acidic vesicles, cells were treated for 2 h prior to fixation with 75 nM Lysotracker Red DND-99 (Life Technologies, L-7528). For assessment of intracellular protease activity, cells were incubated for 4 h prior to fixation with 5 μg ml^{-1} DQ Red-BSA (Life Technologies, D12051).

Where indicated, cells were stained with HCS CellMask Deep Red stain (1:15,000; Life Technologies, H32721) for 30 min and nuclei were counterstained with Hoechst 33342 (1:5,000; Life Technologies, H3570). For confocal microscopy, slides were mounted in Vectashield (VectorLabs, H-1000).

Image acquisition and analysis. For the screenings and time-course experiments, image acquisition was performed using an ImageXpress Micro (Molecular Devices) or Operetta (PerkinElmer) automated high-content screening fluorescence microscope, at ×20 magnification; a total of 16 (ImageXpress Micro) or 9 (Operetta) images were acquired per well or coverslip, corresponding to approximately 2,500 cells analysed per experimental condition and replicate. Image analysis to determine infection rates was performed using the 'multi-wavelength cell scoring' application module implemented in MetaXpress software (Molecular Devices) or custom workflows implemented in Columbus image analysis software (PerkinElmer), as described previously[13,48]. In brief, nuclei and cells were segmented based on Hoechst and CellMask staining, respectively; intracellular bacteria were subsequently identified and cells were classified as positive or negative for *Salmonella* or *Shigella* depending on the total area/intensity of bacterial staining. For binding and early times after infection, results reflect the total number of infected cells, whereas only cells with high bacterial intracellular load, that is cells that presented intracellular bacterial replication, were considered for intermediate and late times after infection.

Quantification of *Shigella* and *Listeria* spreading was performed in Columbus or CellProfiller software[59], essentially as described previously for *Shigella*[48]; taking into account the larger size of *Listeria* infection foci, the analysis of *Listeria* spreading was performed after stitching 9 fields per well, acquired at ×10 magnification. In brief, infection foci were detected on the basis of intensity and/or texture features and the area of individual infection foci were then determined. Infection foci that were small (below 250 μm^2 (*Shigella*) and below 3,500 μm^2 (*Listeria*)) and with low bacterial load were excluded from analysis since they represent non-productive infections; infection foci touching the borders of the images were also excluded to improve the overall accuracy of the measurements. At least 450 (*Shigella*) and 200 (*Listeria*) individual foci from a total of 5 independent experiments were plotted per experimental treatment. *Shigella* Δ*icsA* mutant strain, which is defective in intercellular spreading, was used as a positive control. Custom image analysis workflows implemented in Columbus or CellProfiler image analysis software are available upon request.

Confocal microscopy images, shown as maximum projected *z*-stack images, were acquired with a Leica SP5 laser scanning confocal microscope (Leica Microsystems). For the quantification of bacteria per cell, at least 50 infected cells per condition and independent experiment were counted manually; for the quantification of actin tails in *Shigella* infected cells, at least 200 bacteria per condition and independent experiment were counted manually.

RNA isolation and quantitative reverse transcription PCR . For total RNA isolation, including small RNA fraction, cells were lysed in TRIzol (Life Technologies, 15596026) and RNA was extracted by phenol-chloroform followed by isopropanol precipitation. For the piglet ileum and colon tissue, total RNA was extracted using mirVana miRNA Isolation kit (Invitrogen, AM1561) according to the manufacturer's instructions.

For quantification of gene expression, total RNA was reverse transcribed using hexameric random primers and M-MLV reverse transcriptase (Life Technologies, 28025021), according to the manufacturer's instructions. Quantitative reverse transcription PCR (RT–qPCR) was performed using SsoAdvanced Universal SYBR Green Supermix (BioRad, 172-5274) according to the manufacturer's instructions, using a CFX96 Touch Real-Time PCR detection system (BioRad). The following primer pairs were used: RPL37a, 5′-ATTGAAATCAGCCAGCACGC-3′ and 5′-GCAGGAACCACAGTGCCAGATCC-3′; β-actin, 5′-CCTGTACGCCAACAC AGTGC-3′ and 5′-ATACTCCTGCTTGCTGATCC-3′; RGS2, 5′-AAGTGGCTGC TTTACAAC-3′ and 5′-TACACAAGTCCTGGTAGAAT-3′; N-WASP, 5′-AAGGA TGGGAAACTATTGTGGGA-3′ and 5′- GACGGCCCAAAAGGTCTGTAA-3′. Expression was normalized to β-actin or RPL37a.

For mature miRNA quantification, RNA was reverse transcribed using the miRCURY LNA Universal cDNA synthesis kit (Qiagen, 339340) followed by RT–qPCR using pre-designed miRCURY LNA PCR primer sets (Qiagen) and miRCURY LNA SYBR Green master mix (Qiagen, 339347), according to the manufacturer's instructions, using a CFX96 Touch Real-Time PCR detection system (BioRad). The following primer sets were used: hsa-let-7i-3p and ssc-let-7i-3p (Qiagen, YP0204247), hsa-miR-4732-5p (Qiagen, YP02113664), hsa-miR-6073 (Qiagen, YP02114330), hsa-miR-29a-3p and ssc-miR-29a-3p (Qiagen, YP00204698).

Relative gene expression was calculated using the $-2^{\Delta\Delta C_T}$ method.

Protein extracts and western blot. Cells were washed with PBS, lysed in Laemmli sample buffer, sonicated and separated in 10% SDS–PAGE, followed by western blotting.

For piglet tissue, intestinal sections of about 1 cm^2 were processed as previously described[60]. In brief, mucosa scrapings were homogenized in Laemmli sample buffer containing Proteinase Inhibitor Cocktail (Sigma-Aldrich, P8340) using pre-chilled mortar and pestles, sonicated and centrifuged at 10,000*g* for 15 min. Protein samples were separated by 10% SDS–PAGE, followed by western blotting.

Fractionation of F-actin and G-actin was performed with the G-Actin/F-Actin In Vivo Assay Biochem Kit (Cytoskeleton, BK037), according to the manufacturer's instructions. The quantification of actin in each fraction was performed with ImageJ and used to calculate F-actin:G-actin ratios.

The following antibodies were used: β-actin (1:5,000; Sigma, A2228), RGS2 (1:250; Abcam, ab36561), α-tubulin (1:3,000; Sigma, T6074), GADPH (1:500; GenScript, A01622-40), N-WASP (1:1,000; Cell Signaling Technology, 4848) and anti-mouse and anti-rabbit secondary antibodies coupled to horseradish peroxidase (1:5,000; GE Healthcare, NA931 and NA934, respectively). Signals were detected using SuperSignal West Dura Extended Duration Substrate (Pierce, 34075) using an ImageQuant LAS 4000 CCD camera (GE Healthcare).

Quantification of western blots was performed with ImageJ. Uncropped images of immunoblots are included as Source Data.

GFP and dual-luciferase reporter assay. For the GFP reporter assay, the full coding sequence of RGS2 (ENSG00000116741) and a panel of fragments of the RGS2 coding sequence were amplified by PCR from a HeLa cDNA library and cloned as a C-terminal fusion of the GFP protein in the pEGFP-C1 plasmid (Clontech), between XhoI and BamHI restriction sites. Mutants of let-7i-3p putative binding sites were generated by site-directed mutagenesis. All primers used for cloning and mutagenesis are indicated in Supplementary Table 3. HeLa cells were transfected with control miRNA or let-7i-3p mimic in 24-well plates using a reverse transfection protocol, as described above. Cells were transfected with the RGS2 constructs (EGFP-RGS2 and fragments or mutants) or pEGFP-C1 (empty vector) 24 h after cell seeding and miRNA transfection, using FuGENE HD transfection reagent (Promega, E2311). DsRed-C1 plasmid (Clontech) was co-transfected and used for normalization. Forty-eight hours after plasmid DNA transfection, cells were collected in PBS containing 5 mM EDTA, washed in PBS, fixed in 4% paraformaldehyde for 15 min at room temperature and analysed by flow cytometry. DsRed positive cells (transfected cells) were gated and analysed for GFP fluorescence; a minimum of 15,000 viable cells were analysed per sample. The percentage of double-positive (GFP and DsRed) cells transfected with let-7i-3p mimic was normalized to that of cells transfected with control miRNA for each construct, and then normalized to the results obtained with the control plasmid (empty pEGFP-C1 plasmid).

For the dual-luciferase reporter assay, full length RGS2 and N-WASP 3′UTR were amplified by PCR from a HeLa cDNA library and cloned into the psiCHECK2 reporter vector (Promega, C8021) using XhoI and NotI restriction sites. Mutants of miR-3668, miR-4732-5p and miR-6073 putative binding sites were generated by site directed mutagenesis. All primers used for cloning and mutagenesis are shown in Supplementary Table 3. HeLa-229 cells were seeded 1 d before transfection in 96-well plates (8×10^3 cells per well) and transfected with 200 ng of the constructs containing the wild-type (RGS2 or N-WASP) or mutated sequences (N-WASP) using FuGENE HD transfection reagent (Promega, E2311). Twenty-four hours after plasmid transfection, cells were transfected with control miRNA, let-7i-3p, miR-3668, miR-4732-5p or miR-6073 mimics (final concentration 50 nM) and the experiment was stopped after an additional 48 h period. Firefly and *Renilla* luciferase activities were measured on a VICTOR Light plate reader (PerkinElmer) using the Dual-Luciferase Reporter Assay System (Promega, E1910), according to the manufacturer's instructions. For cells transfected with each miRNA, the ratio of *Renilla*/Firefly luciferase activity was normalized to that of cells transfected with control miRNA, and then normalized to the results obtained with the control plasmid (empty psiCHECK2 plasmid).

RNA sequencing and computational RNA-sequencing analysis. Library preparation and deep sequencing was performed by Vertis Biotechnology, as described previously[13]. RNA-sequencing analysis was performed using the READemption pipeline v.0.3.0 (ref. [61]), with Segemehl v.0.1.7 (ref. [62]). Reads shorter than 14 nt were discarded. Remaining reads were mapped against the human genome (build GRCh37) and *Salmonella* Typhimurium SL1344 (NC_016810.1, NC_017718.1, NC_017719.1 and NC_017720.1). Analysis of differential gene

expression (cells transfected with control miRNA versus let-7i-3p and mock-treated cells versus *Salmonella*-infected cells) was performed with DESeq 1.18.0 (ref. [63]). Only genes with reads >25 for control miRNA and mock-treated cells were considered for the comparison of the genes downregulated in let-7i-3p transfected cells with the genes upregulated on *Salmonella* infection. The demultiplexed FASTQ files and gene-wise quantifications have been deposited in the NCBI Gene Expression Omnibus and are accessible through GEO Series accession numbers GSE53281 (mock-treated and *Salmonella*-infected samples) and GSE69660 (cells transfected with control miRNA or let-7i-3p mimic).

Piglet infections and sample preparation. Nine male and female crossbred weaned piglets, approximately four weeks old, were used in this study; all piglets were serologically negative before the infection. All procedures involving animals were performed at the animal facility of the University of Leon, Spain and were approved by the institutional bioethical committee of the University of Leon, Spain (license number ULE_003_2005, approval date 25 January 2005) and performed according to European regulations regarding animal welfare and protection of animals used for experimental and other scientific purposes. Statistical consideration was not used to determine the animal sample size. Animals were randomly assigned to experimental groups; data blinding was not performed.

Salmonella infection of piglets and sample preparation were performed as described previously[41]. In brief, 6 piglets were challenged orally with 10^8 cfu of *Salmonella* Typhimurium and 3 piglets (mock group) received sterile medium. Necropsies were performed on the mock group before the infection group. Three pigs were necropsied at 2 dpi and three were necropsied at 6 dpi. Sections of mucosal tissue from the ileum and colon were independently sectioned in 10 cm^2 pieces and immediately frozen in liquid nitrogen for protein and RNA isolation.

Statistical analysis. Unless otherwise indicated, data are presented as mean ± s.e.m., with the exact number of experiments performed indicated in the figure legends. Statistical analysis was performed using Prism Software (GraphPad). Normal distribution of the data was assessed by the Shapiro–Wilk test. For statistical comparison of datasets from two conditions, two-tailed Student's *t*-test or multiple *t*-test corrected for multiple comparison using the Holm–Sidak method was used; for data from three or more conditions or groups, one-way ANOVA with Tukey's or Dunnett's post hoc test or two-way ANOVA with Tukey's multiple comparison test was used. For non-parametric data Mann–Whitney or Kruskal–Wallis with Dunn's multiple comparison tests were used. Values of $P < 0.05$ were considered significant. Statistical significance of the overlap between two groups of genes was calculated using hypergeometric probability. Hierarchical clustering of miRNA phenotypes (time-course experiments) was performed on the basis of Euclidean distances using Genesis software[64]. Statistical analyses are detailed in Supplementary Table 4.

Reporting Summary. Further information on research design is available in the Nature Research Reporting Summary linked to this article.

Data availability

The data supporting the findings of this study are available from the corresponding authors upon reasonable request. The demultiplexed FASTQ files and gene-wise quantifications have been deposited in NCBI's Gene Expression Omnibus and are accessible through GEO Series accession numbers GSE53281 (mock-treated and *Salmonella*-infected samples) and GSE69660 (cells transfected with control miRNA or let-7i-3p mimic). Source data for Figs. 3e,i,k, 4f, 5f,g,i and 6h and Extended Data Figs. 3b,d, 5f,h,j and 6b are included in this article and its Supplementary Information files.

Code availability

Custom image analysis workflows implemented in Columbus or CellProfiler image analysis software are available upon reasonable request.

Accepted: 18 October, 2019

References

1. Bartel, D. P. Metazoan microRNAs. *Cell* **173**, 20–51 (2018).
2. Jonas, S. & Izaurralde, E. Towards a molecular understanding of microRNA-mediated gene silencing. *Nat. Rev. Genet.* **16**, 421–433 (2015).
3. Friedman, R. C., Farh, K. K., Burge, C. B. & Bartel, D. P. Most mammalian mRNAs are conserved targets of microRNAs. *Genome Res.* **19**, 92–105 (2009).
4. Aguilar, C., Mano, M. & Eulalio, A. MicroRNAs at the host–bacteria interface: host defense or bacterial offense. *Trends Microbiol.* **27**, 206–218 (2019).
5. Duval, M., Cossart, P. & Lebreton, A. Mammalian microRNAs and long noncoding RNAs in the host-bacterial pathogen crosstalk. *Semin. Cell. Dev. Biol.* **65**, 11–19 (2017).
6. Eulalio, A. & Mano, M. MicroRNA screening and the quest for biologically relevant targets. *J. Biomol. Screen.* **20**, 1003–1017 (2015).
7. Lemons, D., Maurya, M. R., Subramaniam, S. & Mercola, M. Developing microRNA screening as a functional genomics tool for disease research. *Front. Physiol.* **4**, 223 (2013).
8. Rodrigues Lopes, I., Silva, R. J., Caramelo, I., Eulalio, A. & Mano, M. Shedding light on microRNA function via microscopy-based screening. *Methods* **152**, 55–64 (2019).
9. Huang, Q. et al. The microRNAs miR-373 and miR-520c promote tumour invasion and metastasis. *Nat. Cell Biol.* **10**, 202–210 (2008).
10. Eulalio, A. et al. Functional screening identifies miRNAs inducing cardiac regeneration. *Nature* **492**, 376–381 (2012).
11. Judson, R. L., Greve, T. S., Parchem, R. J. & Blelloch, R. MicroRNA-based discovery of barriers to dedifferentiation of fibroblasts to pluripotent stem cells. *Nat. Struct. Mol. Biol.* **20**, 1227–1235 (2013).
12. Santhakumar, D. et al. Combined agonist–antagonist genome-wide functional screening identifies broadly active antiviral microRNAs. *Proc. Natl Acad. Sci. USA* **107**, 13830–13835 (2010).
13. Maudet, C. et al. Functional high-throughput screening identifies the miR-15 microRNA family as cellular restriction factors for *Salmonella* infection. *Nat. Commun.* **5**, 4718 (2014).
14. Collaborators, G. B. D. D. D. Estimates of global, regional, and national morbidity, mortality, and aetiologies of diarrhoeal diseases: a systematic analysis for the Global Burden of Disease Study 2015. *Lancet. Infect. Dis.* **17**, 909–948 (2017).
15. Haselbeck, A. H. et al. Current perspectives on invasive nontyphoidal *Salmonella* disease. *Curr. Opin. Infect. Dis.* **30**, 498–503 (2017).
16. Kotloff, K. L., Riddle, M. S., Platts-Mills, J. A., Pavlinac, P. & Zaidi, A. K. M. Shigellosis. *Lancet* **391**, 801–812 (2018).
17. Steele-Mortimer, O. The *Salmonella*-containing vacuole: moving with the times. *Curr. Opin. Microbiol.* **11**, 38–45 (2008).
18. Mellouk, N. & Enninga, J. Cytosolic access of intracellular bacterial pathogens: the *Shigella* paradigm. *Front. Cell. Infect. Microbiol.* **6**, 35 (2016).
19. Agaisse, H. Molecular and cellular mechanisms of *Shigella flexneri* dissemination. *Front. Cell. Infect. Microbiol.* **6**, 29 (2016).
20. Lambrechts, A., Gevaert, K., Cossart, P., Vandekerckhove, J. & Van Troys, M. *Listeria* comet tails: the actin-based motility machinery at work. *Trends Cell Biol.* **18**, 220–227 (2008).
21. Agarwal, V., Bell, G. W., Nam, J. W. & Bartel, D. P. Predicting effective microRNA target sites in mammalian mRNAs. *eLife* **4**, 05005 (2015).
22. Egile, C. et al. Activation of the CDC42 effector N-WASP by the *Shigella flexneri* IcsA protein promotes actin nucleation by Arp2/3 complex and bacterial actin-based motility. *J. Cell Biol.* **146**, 1319–1332 (1999).
23. Suzuki, T. et al. Neural Wiskott-Aldrich syndrome protein (N-WASP) is the specific ligand for *Shigella* VirG among the WASP family and determines the host cell type allowing actin-based spreading. *Cell. Microbiol.* **4**, 223–233 (2002).
24. Boujemaa-Paterski, R. et al. Listeria protein ActA mimics WASp family proteins: it activates filament barbed end branching by Arp2/3 complex. *Biochemistry* **40**, 11390–11404 (2001).
25. Bierne, H. et al. WASP-related proteins, Abi1 and Ena/VASP are required for *Listeria* invasion induced by the Met receptor. *J. Cell Sci.* **118**, 1537–1547 (2005).
26. Lara-Tejero, M. & Galan, J. E. *Salmonella enterica* serovar Typhimurium pathogenicity island 1-encoded type III secretion system translocases mediate intimate attachment to nonphagocytic cells. *Infect. Immun.* **77**, 2635–2642 (2009).
27. Misselwitz, B. et al. *Salmonella enterica* serovar Typhimurium binds to HeLa cells via Fim-mediated reversible adhesion and irreversible type three secretion system 1-mediated docking. *Infect. Immun.* **79**, 330–341 (2011).
28. Schlumberger, M. C. et al. Real-time imaging of type III secretion: *Salmonella* SipA injection into host cells. *Proc. Natl Acad. Sci. USA* **102**, 12548–12553 (2005).
29. Menard, R., Sansonetti, P. J. & Parsot, C. Nonpolar mutagenesis of the *ipa* genes defines IpaB, IpaC, and IpaD as effectors of *Shigella flexneri* entry into epithelial cells. *J. Bacteriol.* **175**, 5899–5906 (1993).
30. Woodard, G. E., Jardin, I., Berna-Erro, A., Salido, G. M. & Rosado, J. A. Regulators of G-protein-signaling proteins: negative modulators of G-protein-coupled receptor signaling. *Int. Rev. Cell Mol. Biol.* **317**, 97–183 (2015).
31. Sethakorn, N., Yau, D. M. & Dulin, N. O. Non-canonical functions of RGS proteins. *Cell. Signal.* **22**, 1274–1281 (2010).
32. Tuli, A. & Sharma, M. How to do business with lysosomes: *Salmonella* leads the way. *Curr. Opin. Microbiol.* **47**, 1–7 (2018).
33. Garcia-del Portillo, F. & Finlay, B. B. Targeting of *Salmonella typhimurium* to vesicles containing lysosomal membrane glycoproteins bypasses compartments with mannose 6-phosphate receptors. *J. Cell Biol.* **129**, 81–97 (1995).
34. Rathman, M., Barker, L. P. & Falkow, S. The unique trafficking pattern of *Salmonella typhimurium*-containing phagosomes in murine macrophages is independent of the mechanism of bacterial entry. *Infect. Immun.* **65**, 1475–1485 (1997).
35. Santos, J. C. et al. The COPII complex and lysosomal VAMP7 determine intracellular *Salmonella localization* and growth. *Cell. Microbiol.* **17**, 1699–1720 (2015).

36. Hang, H. C. et al. Mechanism-based probe for the analysis of cathepsin cysteine proteases in living cells. *ACS Chem. Biol.* **1**, 713–723 (2006).
37. Meresse, S., Steele-Mortimer, O., Finlay, B. B. & Gorvel, J. P. The rab7 GTPase controls the maturation of *Salmonella typhimurium*-containing vacuoles in HeLa cells. *EMBO J.* **18**, 4394–4403 (1999).
38. Brown, W. J., DeWald, D. B., Emr, S. D., Plutner, H. & Balch, W. E. Role for phosphatidylinositol 3-kinase in the sorting and transport of newly synthesized lysosomal enzymes in mammalian cells. *J. Cell Biol.* **130**, 781–796 (1995).
39. Davidson, H. W. Wortmannin causes mistargeting of procathepsin D. Evidence for the involvement of a phosphatidylinositol 3-kinase in vesicular transport to lysosomes. *J. Cell Biol.* **130**, 797–805 (1995).
40. Gaffet, P., Jones, A. T. & Clague, M. J. Inhibition of calcium-independent mannose 6-phosphate receptor incorporation into *trans*-Golgi network-derived clathrin-coated vesicles by wortmannin. *J. Biol. Chem.* **272**, 24170–24175 (1997).
41. Ikeda, K. et al. Drug-induced phospholipidosis is caused by blockade of mannose 6-phosphate receptor-mediated targeting of lysosomal enzymes. *Biochem. Biophys. Res. Commun.* **377**, 268–274 (2008).
42. Reaves, B. J., Bright, N. A., Mullock, B. M. & Luzio, J. P. The effect of wortmannin on the localisation of lysosomal type I integral membrane glycoproteins suggests a role for phosphoinositide 3-kinase activity in regulating membrane traffic late in the endocytic pathway. *J. Cell Sci.* **109**, 749–762 (1996).
43. Brumell, J. H., Tang, P., Zaharik, M. L. & Finlay, B. B. Disruption of the *Salmonella*-containing vacuole leads to increased replication of *Salmonella enterica* serovar typhimurium in the cytosol of epithelial cells. *Infect. Immun.* **70**, 3264–3270 (2002).
44. Collado-Romero, M., Arce, C., Ramirez-Boo, M., Carvajal, A. & Garrido, J. J. Quantitative analysis of the immune response upon *Salmonella typhimurium* infection along the porcine intestinal gut. *Vet. Res.* **41**, 23 (2010).
45. Denzler, R. et al. Impact of microRNA levels, target-site complementarity, and cooperativity on competing endogenous RNA-regulated gene expression. *Mol. Cell* **64**, 565–579 (2016).
46. Hon, L. S. & Zhang, Z. The roles of binding site arrangement and combinatorial targeting in microRNA repression of gene expression. *Genome Biol.* **8**, R166 (2007).
47. Campellone, K. G. & Welch, M. D. A nucleator arms race: cellular control of actin assembly. *Nat. Rev. Mol. Cell Biol.* **11**, 237–251 (2010).
48. Sunkavalli, U. et al. Analysis of host microRNA function uncovers a role for miR-29b-2-5p in *Shigella* capture by filopodia. *PLoS Pathog.* **13**, e1006327 (2017).
49. Hume, P. J., Singh, V., Davidson, A. C. & Koronakis, V. Swiss Army pathogen: the *Salmonella* entry toolkit. *Front. Cell. Infect. Microbiol.* **7**, 348 (2017).
50. Van Nhieu, G. T. & Romero, S. Common themes in cytoskeletal remodeling by intracellular bacterial effectors. *Handb. Exp. Pharmacol.* **235**, 207–235 (2017).
51. Sullivan, B. M. et al. RGS4 and RGS2 bind coatomer and inhibit COPI association with Golgi membranes and intracellular transport. *Mol. Biol. Cell* **11**, 3155–3168 (2000).
52. McGourty, K. et al. *Salmonella* inhibits retrograde trafficking of mannose-6-phosphate receptors and lysosome function. *Science* **338**, 963–967 (2012).
53. Tawk, C. et al. Stress-induced host membrane remodeling protects from infection by non-motile bacterial pathogens. *EMBO J.* **37**, e98529 (2018).
54. Papenfort, K. et al. Specific and pleiotropic patterns of mRNA regulation by ArcZ, a conserved, Hfq-dependent small RNA. *Mol. Microbiol.* **74**, 139–158 (2009).
55. Eulalio, A., Frohlich, K. S., Mano, M., Giacca, M. & Vogel, J. A candidate approach implicates the secreted *Salmonella* effector protein SpvB in P-body disassembly. *PLoS ONE* **6**, e17296 (2011).
56. Garcia-Feliz, C. et al. *Salmonella enterica* infections in Spanish swine fattening units. *Zoonoses Public Health* **54**, 294–300 (2007).
57. Hussain, N. K. et al. Endocytic protein intersectin-l regulates actin assembly via Cdc42 and N-WASP. *Nat. Cell Biol.* **3**, 927–932 (2001).
58. Sancak, Y. et al. The Rag GTPases bind raptor and mediate amino acid signaling to mTORC1. *Science* **320**, 1496–1501 (2008).
59. McQuin, C. et al. CellProfiler 3.0: Next-generation image processing for biology. *PLoS Biol.* **16**, e2005970 (2018).
60. Collado-Romero, M. et al. Quantitative proteomics and bioinformatic analysis provide new insight into the dynamic response of porcine intestine to *Salmonella Typhimurium*. *Front. Cell. Infect. Microbiol.* **5**, 64 (2015).
61. Forstner, K. U., Vogel, J. & Sharma, C. M. READemption-a tool for the computational analysis of deep-sequencing-based transcriptome data. *Bioinformatics* **30**, 3421–3423 (2014).
62. Otto, C., Stadler, P. F. & Hoffmann, S. Lacking alignments? The next-generation sequencing mapper segemehl revisited. *Bioinformatics* **30**, 1837–1843 (2014).
63. Anders, S. & Huber, W. Differential expression analysis for sequence count data. *Genome Biol.* **11**, R106 (2010).
64. Sturn, A., Quackenbush, J. & Trajanoski, Z. Genesis: cluster analysis of microarray data. *Bioinformatics* **18**, 207–208 (2002).

Acknowledgements

C.A. is a recipient of a fellowship from the Bayerischen Gleichstellungsförderung (BGF) through the SCIENTIA Program; I.R.L. and R.J.S. are recipients of PhD fellowships (PD/BD/146464/2019 and PD/BD/129294/2017) of the Doctoral Programme in Experimental Biology and Biomedicine of the Center for Neuroscience and Cell Biology, University of Coimbra. The authors acknowledge the animal facility staff at the University of Leon, Spain, in particular A. Carvajal from the Department of Animal Health. This work was supported by grants from the Bavarian Ministry of Sciences, Research and the Arts in the framework of the Bavarian Molecular Biosystems Research Network (BioSysNet), DFG project BR 4837/1-1 and the Portuguese Foundation for Science and Technology (FCT Investigator Programme IF/01105/2015).

Author contributions

C.A., A.R.C., C.M., M.M. and A.E. designed the experiments; A.R.C., M.M. and A.E. performed the high-throughput screening and validation experiments; C.A., I.R.L., C.M., U.S., R.J.S. and C.L. performed the biochemical and cell biology assays for characterization of the role of miRNAs in infection; M.S. performed the analysis of the RNA-sequencing datasets; S.Z.-L. and J.J.G. performed the in vivo *Salmonella* infections; M.G. provided reagents and access to equipment; M.M. and A.E. wrote the manuscript, with input from all authors.

Competing interests

The authors declare no competing interests.

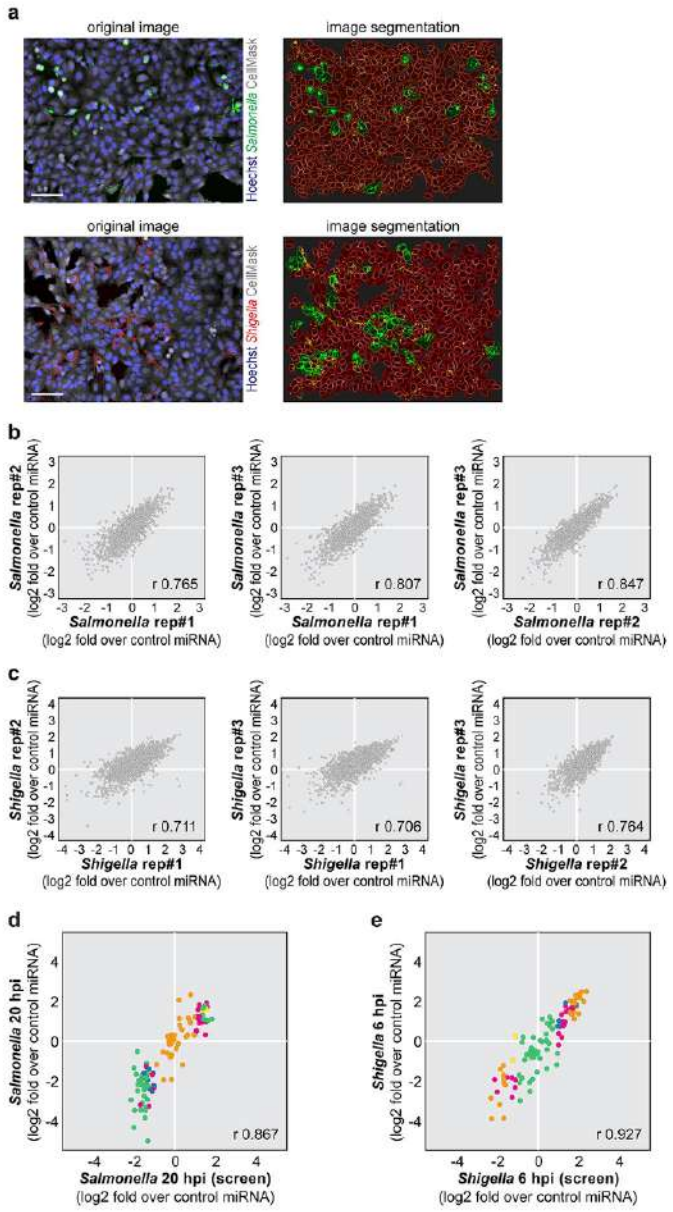

Extended Data Fig. 1 | Screenings for miRNAs controlling infection by *Salmonella* and *Shigella*. a. Microscopy images and corresponding image segmentation outlines of HeLa cells treated with control miRNA and infected with *Salmonella* or *Shigella*. Cells marked in green in the image segmentation panels correspond to cells with high intracellular bacterial load; cells touching the borders of the images were excluded from the analysis. Scale bar, 100 µm. **b** and **c**. Pairwise correlation between the three independent runs of the screenings to identify miRNAs that regulate *Salmonella* (**b**) and *Shigella* (**c**) infection. Results are based on quantification of the percentage of infected cells following treatment with the library of miRNA mimics and are shown as fold change compared to control miRNA (log2 scale). Spearman rank correlation coefficients are shown in the right bottom corner of graphs. **d** and **e**. Comparison of the results obtained in the *Salmonella* (**d**) and *Shigella* (**e**) screenings for the 110 selected miRNAs, with those obtained for the corresponding time point in the time-course experiments (20 hpi, *Salmonella*; 6 hpi, *Shigella*). Results shown are the mean of the three independent runs of each screen or time-course experiments. Colours in panels **d** and **e** correspond to the different miRNA categories identified in Figure 2a. Spearman rank correlation coefficients are shown in the right bottom corner of graphs.

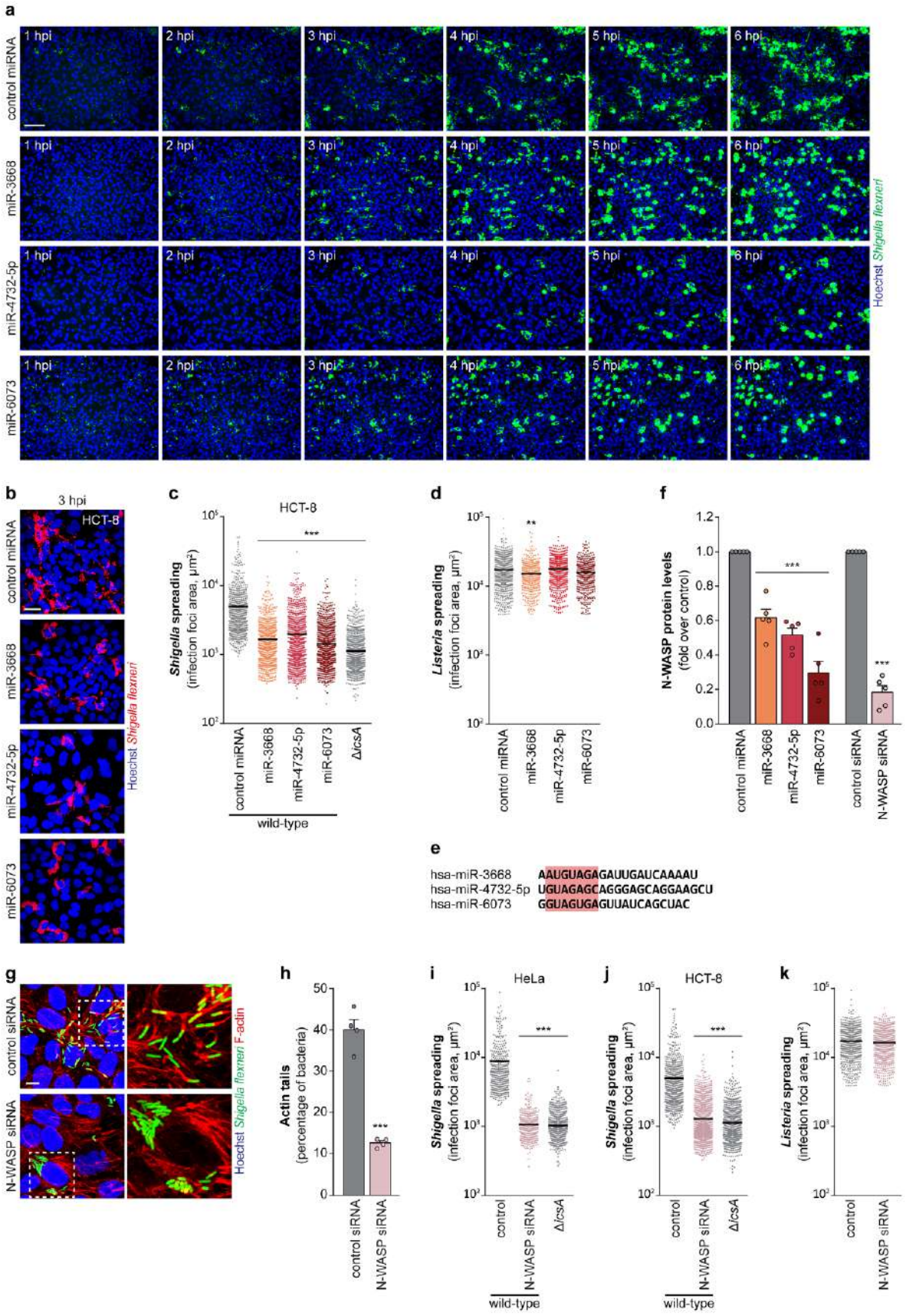

Extended Data Fig. 2 | See next page for caption.

Extended Data Fig. 2 | *Shigella* intracellular motility and intercellular spreading are inhibited by miR-3668, miR-4732-5p and miR-6073. a. Fluorescence microscopy images extracted from the time-lapse microscopy analysis of HeLa cells infected with *Shigella* wild-type, upon treatment with control miRNA, miR-3668, miR-4732-5p or miR-6073 mimics. Full time-lapse sequence is included as Supplementary Videos 1-4. Scale bar, 100 µm. **b** and **c**. Representative images (**b**) and area of *Shigella* infection foci (**c**) in HCT-8 cells transfected with control miRNA, miR-3668, miR-4732-5p or miR-6073 mimics and infected with *Shigella*, analyzed at 3 hpi. *Shigella* Δ*icsA* mutant is shown for comparison. Scale bar, 25 µm. **d**. Area of *Listeria* infection foci in HeLa cells transfected with the indicated miRNAs, analyzed at 8 hpi. **e**. Sequences of mature human miR-3668, miR-4732-5p and miR-6073. The 7-mer seed sequences of the miRNAs are highlighted in red. **f**. N-WASP levels, determined by western blot, in HeLa cells transfected with control miRNA, miR-3668, miR-4732-5p or miR-6073 mimics, or with control siRNA or N-WASP siRNA. **g** and **h**. Representative images (**g**) and percentage of bacteria forming actin tails (**h**) in HeLa cells transfected with control siRNA or N-WASP siRNA, analyzed at 1.5 hpi. Staining of F-actin using fluorescently labeled phalloidin allows the visualization of actin tails. Scale bar, 10 µm. **i** and **j**. Area of *Shigella* infection foci in HeLa (**i**) and HCT-8 (**j**) cells transfected with control miRNA or N-WASP siRNA, analyzed at 3 hpi. *Shigella* Δ*icsA* mutant is shown for comparison. **k**. Area of *Listeria* infection foci in HeLa cells transfected with control miRNA or N-WASP siRNA, analyzed at 3 hpi. *Shigella* infection was performed at MOI 25 (**b**,**g**,**h**), 10 (**a**,**i**) or 5 (**c**,**j**); *Listeria* infection was performed at MOI 20. Results are shown as mean ± s.e.m. of n=4 (**h**) or n=5 (**c**,**f**,**i-k**) biologically independent experiments; microscopy images are representative of n=3 (a), n=4 (**g**) or n=5 (**b**) biologically independent experiments; centre values indicate means (**c**,**d**,**h-j**); ***P<0.001 (statistical analyses are detailed in Supplementary Table 4).

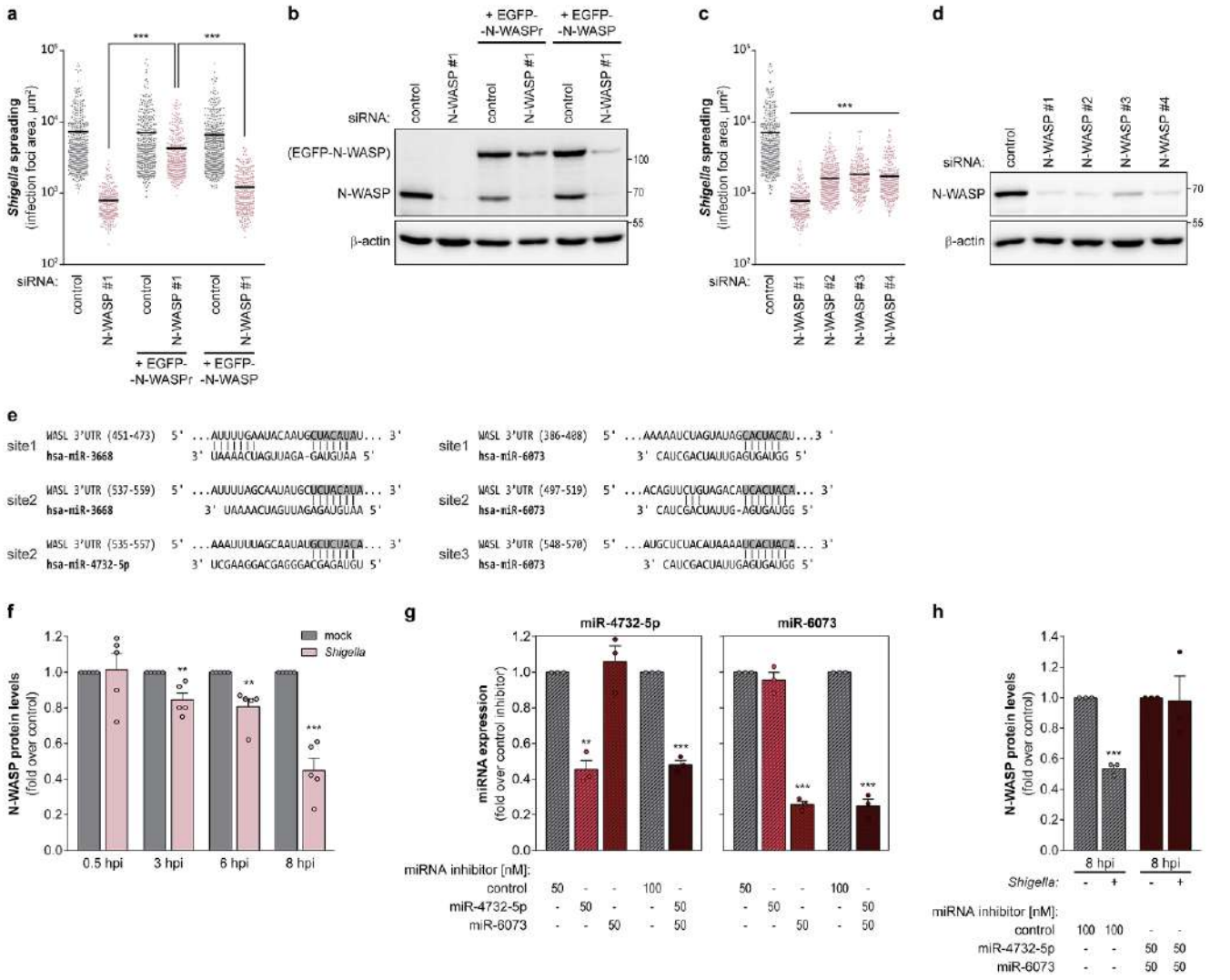

Extended Data Fig. 3 | Targeting of N-WASP by miR-3668, miR-4732-5p and miR-6073 inhibits *Shigella* intercellular spreading. a. Area of *Shigella* infection foci (in parental HeLa cells, HeLa cells stably expressing a siRNA resistant version of N-WASP fused with EGFP (EGFP-N-WASPr) or wild-type N-WASP fused with EGFP (EGFP-N-WASP), transfected with a control siRNA or a siRNA targeting N-WASP, analyzed at 3 hpi. **b**. N-WASP expression, determined by western blot, in HeLa cells (parental, EGFP-N-WASPr, EGFP-N-WASP) transfected with a control siRNA or a siRNA targeting N-WASP. **c**. Area of *Shigella* infection foci in HeLa cells transfected with control siRNA or 4 independent siRNAs targeting N-WASP, analyzed at 3 hpi. **d**. N-WASP expression, determined by western blot, in HeLa cells transfected with control siRNA or 4 independent siRNAs targeting N-WASP. **e**. Sequences of the six active binding sites for miR-3668 (2 sites), miR-4732-5p (1 site) and miR-6073 (3 sites) identified in the 3'UTR of N-WASP. Complementarity of the binding sites with the miRNAs, as predicted by TargetScan, is shown. **f**. N-WASP levels, determined by western blot, in HeLa cells mock-treated or infected with *Shigella*, at different times post-infection (0.5, 3, 6 and 8 hpi). **g**. Expression of mature miR-4732-5p or miR-6073, determined by RT-qPCR, in HeLa cells transfected with control miRNA inhibitor or inhibitors of miR-4732-5p and miR-6073, separately or simultaneously. **h**. N-WASP levels, determined by western blot, in HeLa cells mock-treated or infected with *Shigella*, and transfected with control miRNA inhibitor or inhibitors of miR-4732-5p and miR-6073 simultaneously, analyzed at 8 hpi. *Shigella* infection was performed at MOI 100 (**f**,**h**) or 10 (**a**,**c**). Results are shown as mean ± s.e.m. of n=3 (**g**,**h**) or n=5 (**a**,**c**,**f**) biologically independent experiments; western blots (**b**,**d**) are representative of n=3 biologically independent experiments; centre values indicate means (**a**,**d**); **P<0.01, ***P<0.001 (statistical analyses are detailed in Supplementary Table 4).

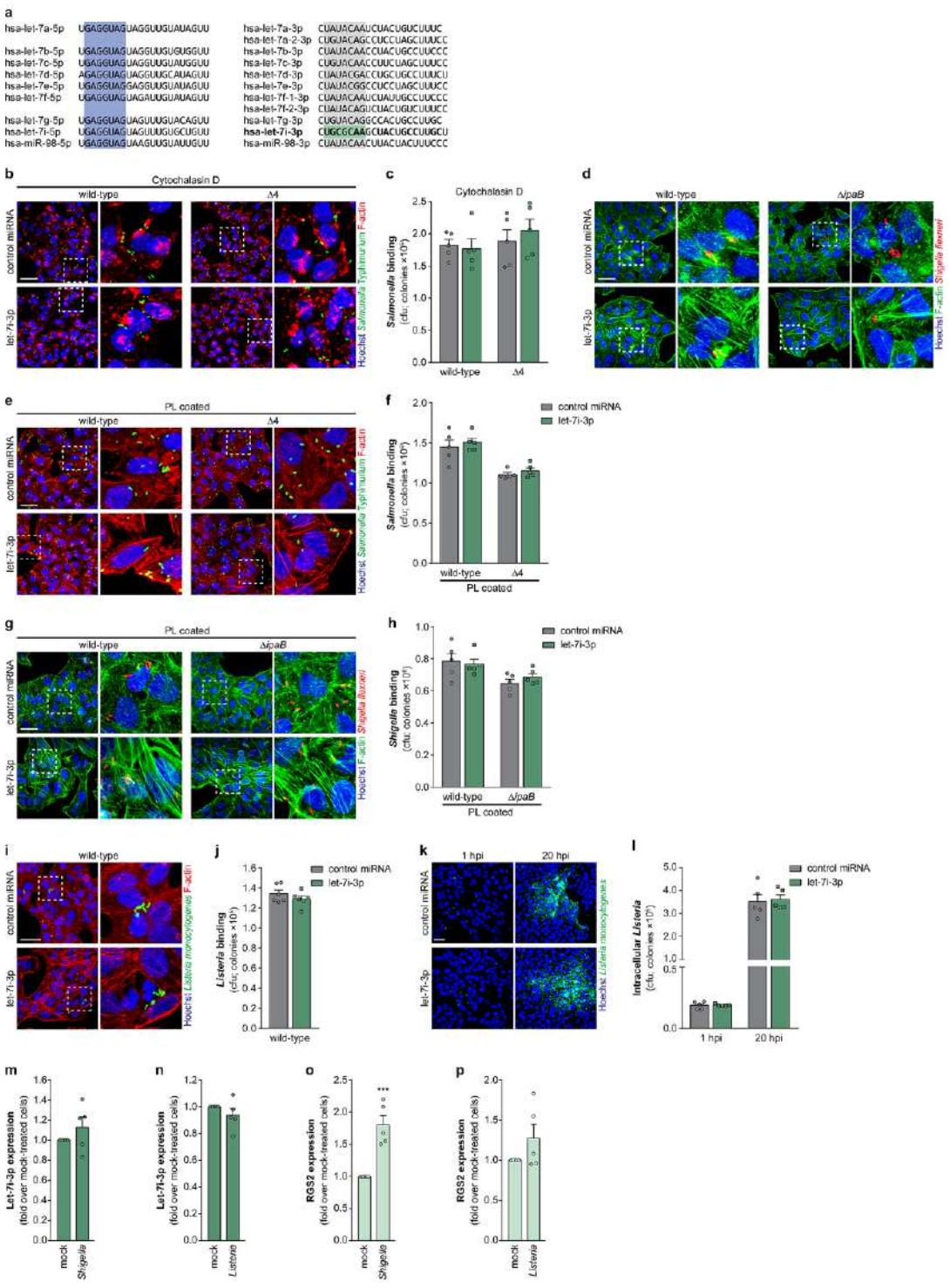

Extended Data Fig. 4 | Disruption of actin stress fibers reverts the inhibitory effect of let-7i-3p on *Salmonella* binding to host cells. a. Sequences of the mature miRNAs derived from the 5' and 3' arm of the precursors of the let-7 family. Common seed sequence of the let-7 miRNA family (-5p miRNAs) is highlighted in blue and that of let-7i-3p is highlighted in green. **b**, **c**, **e** and **f**. Representative images (**b**,**e**) and quantification by cfu (**c**,**f**) of *Salmonella* bound to HeLa cells transfected with control miRNA or let-7i-3p mimics, and incubated with *Salmonella* wild-type or Δ4 mutant strain for 10 min. Cells were pre-treated with cytochalasin D for 1 h (**b**,**c**). *Salmonella* was previously coated with PL (**e**,**f**). **d**, **g** and **h**. Representative images (**d**,**g**) and quantification by cfu (**h**) of *Shigella* bound to HeLa cells transfected with control miRNA or let-7i-3p mimics, and incubated with *Shigella* wild-type or Δ*ipaB* mutant strains for 25 min. *Shigella* was previously coated with PL (g,h). **i-l**. Representative images (**i**,**k**) and quantification by cfu (**j**,**l**) of *Listeria* bound to (**i**,**j**) or intracellular *Listeria* (**k**,**l**) of HeLa cells transfected with control miRNA or let-7i-3p mimics. Binding was performed for 25 min, and intracellular bacteria analyzed at 1 and 20 hpi. **m-p**. Expression of mature let-7i-3p (**m**,**n**) and RGS2 (**o**,**p**), evaluated by RT-qPCR, in HeLa cells infected with *Shigella* (**m**,**o**) or *Listeria* (**n**,**p**). *Shigella* and *Listeria* infections were analyzed at 6 or 20 hpi, respectively. *Salmonella* infection was performed at MOI 50. *Shigella* infection was performed at MOI 50 (**d**,**g**,**h**) or MOI 100 (**m**,**o**). *Listeria* infection was performed at MOI 25 (**k**,**l**,**n**,**p**) or 50 (**i**,**j**). Scale bars, 50 μm. Results are shown as mean ± s.e.m. of n=5 (**c**,**f**,**h**,**l**-**p**) or n=6 (**j**) biologically independent experiments; microscopy images are representative of n=3 (**i**,**k**) or n=5 (**b**,**d**,**e**,**g**) biologically independent experiments; ***P<0.001 (statistical analyses are detailed in Supplementary Table 4).

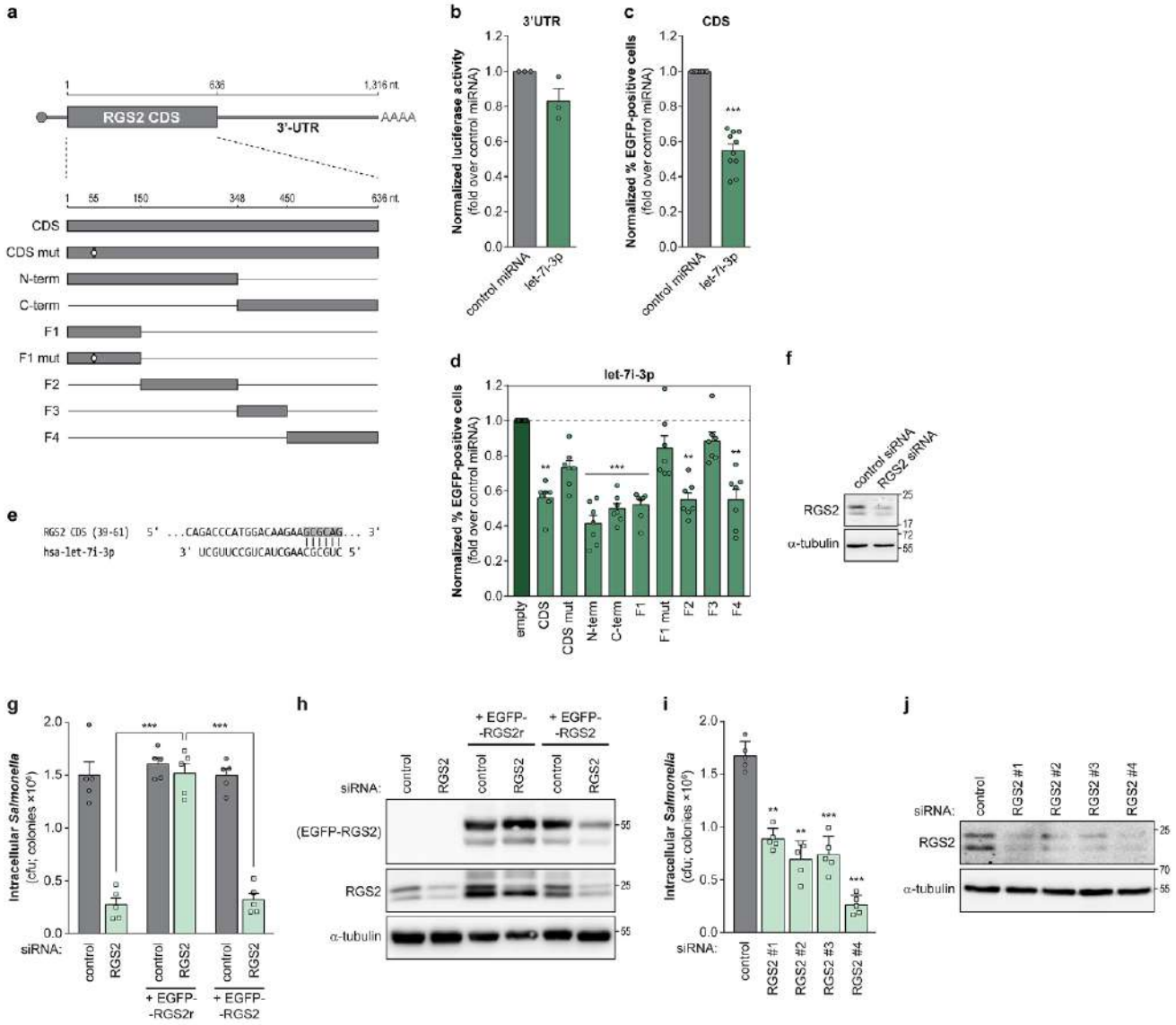

Extended Data Fig. 5 | Let-7i-3p targets the coding sequence of RGS2. a. Schematic representation of RGS2 3'UTR, CDS, and CDS fragments and mutant constructs used for miRNA binding site reporter assays. The RGS2 3'UTR was cloned downstream of a Renilla luciferase reporter (psiCHECK2-RGS2 3'UTR) and the RGS2 CDS and CDS fragments were cloned as a C-terminal fusion of green fluorescent protein (EGFP-RGS2 CDS). **b**-**d**. Results of the reporter assays using the RGS2 3'UTR (**b**), RGS2 CDS (**c**), or RGS2 CDS fragments and mutant (**d**). Results in cells treated with the let-7i-3p mimic are shown compared to the control miRNA. **e**. Sequence of the binding site for let-7i-3p in fragment F1 of the N-WASP CDS. Complementarity of the miRNA with the binding site of human RGS2 sequence is shown. **f**. RGS2 expression, determined by western blot, in HeLa cells transfected with control siRNA or RGS2 siRNA. **g**. Quantification of intracellular *Salmonella* by cfu in parental HeLa cells, HeLa cells stably expressing a siRNA resistant version of RGS2 fused with EGFP (EGFP-RGS2r) or wild-type RGS2 fused with EGFP (EGFP-RGS2), transfected with a control siRNA or a siRNA targeting RGS2, analyzed at 20 hpi. **h**. RGS2 expression, determined by western blot, in HeLa cells (parental, EGFP-RGS2r or EGFP-RGS2), transfected with a control siRNA or a siRNA targeting RGS2. **i**. Quantification of intracellular *Salmonella* by cfu in HeLa cells transfected with control siRNA or 4 independent siRNAs targeting RGS2, analyzed at 20 hpi. **j**. RGS2 expression, determined by western blot, in HeLa cells transfected with control siRNA or 4 independent siRNAs targeting RGS2. *Salmonella* infection was performed at MOI 25. Results are shown as mean ± s.e.m. of n=3 (**b**), n=5 (**g**,**i**), n=7 (**d**) or n=10 (**c**) biologically independent experiments; western blots (**f**,**h**,**j**) are representative of n=3 biologically independent experiments; **P<0.01, ***P<0.001 (statistical analyses are detailed in Supplementary Table 4).

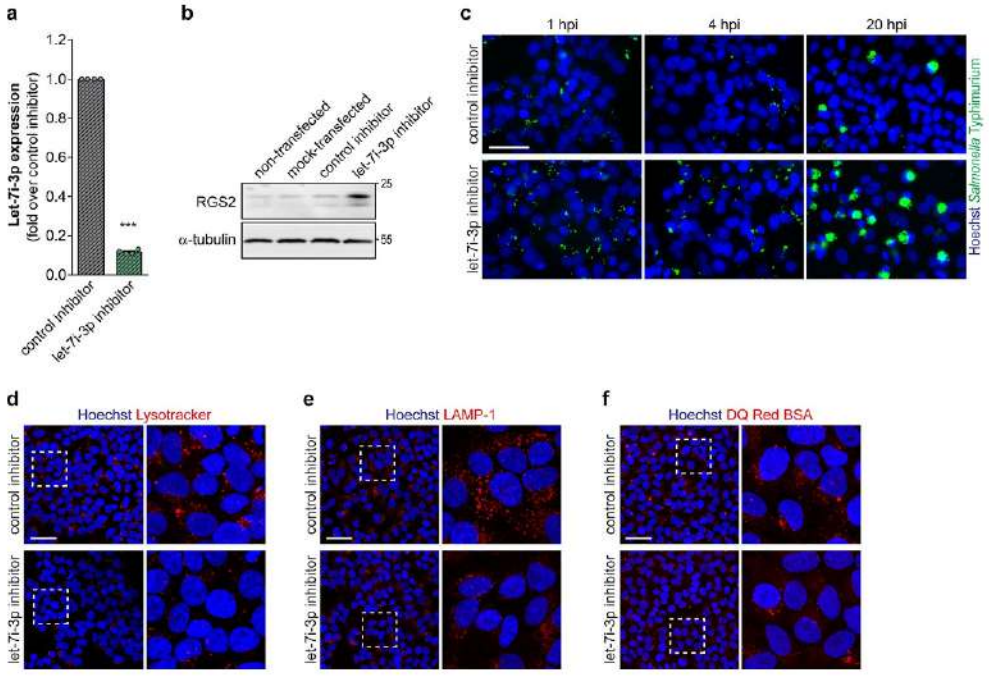

Extended Data Fig. 6 | Inhibition of let-7i-3p favours *Salmonella* infection. a. Expression of mature let-7i-3p, determined by RT-qPCR, in HeLa cells transfected with control miRNA or let-7i-3p inhibitors. **b**. RGS2 expression, determined by western blot, in HeLa cells transfected with control miRNA or let-7i-3p inhibitors; non-transfected and mock-transfected cells are shown for comparison. **c**. Representative images of HeLa cells transfected with control miRNA or let-7i-3p inhibitors and infected with *Salmonella*. Infection was analyzed at 1, 4 and 20 hpi. *Salmonella* infection was performed at MOI 25. Scale bar, 50 µm. **d**-**f**. Representative images of HeLa cells transfected with control miRNA or let-7i-3p inhibitors and stained with Lysotracker (**d**), for LAMP-1 (**e**), or with DQ Red BSA (**f**). Scale bar, 50 µm. Results are shown as mean ± s.e.m. of n=4 (**a**) biologically independent experiments; western blots and microscopy images are representative of n=3 (**b**,**d**-**f**) or n=5 (**c**) biologically independent experiments; ***P<0.001 (statistical analyses are detailed in Supplementary Table 4).